Advances in Physics: X

ISSN: 2374-6149 (Online) Journal homepage: www.tandfonline.com/journals/tapx20

Achromatic multi-level diffractive lenses and related applications

Yanhao Chu, Xiaopeng Li, Xingjian Xiao, Shining Zhu & Tao Li

To cite this article: Yanhao Chu, Xiaopeng Li, Xingjian Xiao, Shining Zhu & Tao Li (2025) Achromatic multi-level diffractive lenses and related applications, Advances in Physics: X, 10:1, 2580626, DOI: 10.1080/23746149.2025.2580626

To link to this article: https://doi.org/10.1080/23746149.2025.2580626

Published online: 11 Nov 2025.

ADVANCES IN PHYSICS: X
2025, VOL. 10, NO. 1, 2580626
https://doi.org/10.1080/23746149.2025.2580626

Taylor & Francis
Taylor & Francis Group

REVIEW ARTICLE

OPEN ACCESS Check for updates

Achromatic multi-level diffractive lenses and related applications

Yanhao Chu, Xiaopeng Li, Xingjian Xiao, Shining Zhu and Tao Li

National Laboratory of Solid State Microstructures, Key Laboratory of Intelligent Optical Sensing and Manipulation, Jiangsu Key Laboratory of Artificial Functional Materials, Collaborative Innovation Center of Advanced Microstructures, College of Engineering and Applied Sciences, Nanjing University, Nanjing, People's Republic of China

ABSTRACT

Achromatic multilevel diffractive lenses (AMDLs) represent a breakthrough in flat optics by overcoming chromatic aberration with practical manufacturability. This review examines their evolution from concepts to state-of-the-art devices (2016–2025), analyzing design methods, fabrication, limitations, and applications. We trace the development from zone plates to free-form AMDLs, highlighting the shift from analytical to computational design. The review explores inverse optimization algorithms like direct binary search and global optimization for achieving broadband achromatic performance. Manufacturing advances are categorized, from lithography for centimeter-scale devices to emerging techniques such as 3D printing and laser direct writing. Theoretical analysis establishes fundamental trade-offs between lens diameter, numerical aperture, bandwidth, and efficiency. We compare AMDLs with achromatic metalenses to outline the advantages and trade-offs of each paradigm. Furthermore, we examine the integration of artificial intelligence in AMDL design, from correction algorithms to end-to-end optimization. This synergy of computational optics, advanced manufacturing, and machine learning enables compact, high-performance optical systems for consumer electronics, scientific instrumentation, and photonic technologies, providing engineers with key insights and future research directions.

ARTICLE HISTORY
Received 24 June 2025
Accepted 22 October 2025

KEYWORDS
Achromatic multilevel diffractive lenses (AMDLs); flat optics; chromatic aberration correction; diffractive optical elements (DOEs); inverse design optimization; deep learning.

1. Introduction

Optical lenses serve as fundamental components across diverse technological domains, from consumer electronics and scientific instrumentation to advanced manufacturing and telecommunications systems. However, chromatic aberration—the wavelength-dependent variation in focal length—remains one of the most persistent challenges in optical system design. This phenomenon, which fundamentally arises from material dispersion in refractive elements and the wavelength-dependence of optical path in diffractive elements, manifests as image blurring, color fringing, and reduced resolution, affecting applications ranging from smartphone cameras to high-end microscopy systems. As modern applications increasingly demand compact, lightweight, and high-performance optical systems, the development of efficient achromatic solutions has become more critical than ever.

Traditional refractive optics has achieved remarkable success in chromatic aberration correction through sophisticated material engineering and multi-element designs. The classical approach relies on combining different optical materials with complementary dispersion characteristics to achieve color correction [1]. However, these solutions face fundamental limitations imposed by the finite range of available optical materials and their inherent dispersion properties. Multi-element designs inevitably increase system complexity, weight, and cost, while residual chromatic aberrations remain challenging to eliminate completely, particularly in high-numerical-aperture systems requiring broad spectral coverage.

CONTACT Tao Li taoli@nju.edu.cn National Laboratory of Solid State Microstructures, Key Laboratory of Intelligent Optical Sensing and Manipulation, Jiangsu Key Laboratory of Artificial Functional Materials, Collaborative Innovation Center of Advanced Microstructures, College of Engineering and Applied Sciences, Nanjing University, Nanjing 210093, People's Republic of China

The emergence of flat optics [2–4] has revolutionized optical design paradigms, offering unprecedented opportunities to overcome traditional limitations while meeting the stringent demands of modern miniaturized systems. Planar optical elements provide compelling advantages including ultra-thin profiles compatible with semiconductor manufacturing processes, reduced alignment complexity, and the potential for monolithic integration with electronic components. Among these, multilevel diffractive lenses (MDL) represent a major class of flat optical elements that achieve focusing by encoding discrete phase delays across their aperture. Broadly speaking, these lenses can be grouped into two distinct technological pathways based on their underlying mechanism for phase modulation. One pathway relies on subwavelength nanostructures, commonly known as metalenses [5–11], where local phase shifts are imparted through geometric phase, Mie resonances, or hybrid mechanisms at the nanoscale. The other pathway modulates phase by varying the physical height—and thus the optical path length—of a dielectric material across the surface.

Significant progress has been made in achromatic performance within both technological branches. In the case of metalenses, researchers have demonstrated various strategies for chromatic correction. These include designs that achieve achromatism at continuous broadband [12–17], discrete wavelengths [18] operation across the visible [12–18] or infrared spectrum [19,20], and configurations that maintain high efficiency [21] and high numerical aperture [22], albeit often constrained by small aperture sizes [23–25] or reliance on complex multi-layer architectures [26,27]. In parallel, the field of thickness-modulated diffractive lenses [9,28–33] has undergone its own evolution. Early implementations often combined diffractive profiles with refractive elements [34–38] or employed harmonic diffractive designs [39,40] with inherently limited bandwidth. A pivotal advancement occurred in 2016 [41] with the introduction of freeform, inverse-designed AMDLs. By computationally optimizing continuous height profiles without analytical constraints, this approach unlocked unprecedented broadband achromatic performance—spanning from the visible to the infrared—while remaining compatible with scalable microfabrication and emerging printing technologies.

Notably, the field of achromatic metalenses has been extensively reviewed in several high-quality publications [42–46], which comprehensively cover their design principles, fabrication techniques, and diverse applications. In contrast, a systematic and up-to-date review focusing specifically on the rapidly advancing domain of achromatic diffractive lenses based on thickness modulation is currently lacking. Therefore, this review aims to fill this critical gap by providing a comprehensive overview of AMDLs grounded in the thickness-modulation paradigm. We systematically examine the evolution of design methodologies, from conventional analytical approaches to advanced inverse optimization and machine learning-driven co-design. We also detail recent breakthroughs in fabrication technologies, ranging from traditional lithography to additive and large-scale printing methods, and discuss their impact on device performance and scalability. And we analyze the fundamental performance limitations and inherent trade-offs of this platform. As both technological branches are promising candidates for flat optics applications with many shared characteristics, we present a detailed comparison between metalenses and MDLs to offer a more holistic and systematic understanding of their respective strengths and constraints. Furthermore, we explore the integration of artificial intelligence (AI) and machine learning approaches that are beginning to accelerate AMDL design processes and enable novel functionalities. Our goal is to equip researchers and engineers with a clear understanding of the state of the art and to identify promising future directions, thereby accelerating the innovation and practical adoption of this transformative technology in the broader landscape of flat optics.

2. Evolution of diffractive lens technologies: from zone plates to free-form AMDLs

The development of diffractive lens technologies represents a fascinating journey from simple binary structures to sophisticated free-form designs, driven by the persistent challenge of chromatic aberration and the quest for improved optical performance. This evolution spans over two centuries, from Fresnel's theoretical foundations to modern computational optimization approaches that enable unprecedented achromatic capabilities.

2.1. Fresnel zone plates: the foundation of diffractive optics

Fresnel zone plates represent the earliest practical implementation of diffractive focusing elements, consisting of alternating opaque and transparent concentric rings designed to constructively interfere at a specific focal point, as shown in Figure 1(a). The radius of the $i\ th$ zone is given by $r_n = \sqrt{(i\lambda f)}$, where λ is the wavelength and f is the focal length. This simple binary structure achieves focusing through diffraction rather than refraction, eliminating the need for curved surfaces.

The fundamental limitation of zone plates lies in their inherently low efficiency. The theoretical maximum efficiency for the first-order focus is only 10.1%, with significant power distributed among unwanted higher-order foci at distances f/m (where$m = \pm1, \pm2, \pm3\ldots$) as shown in Figure 1(f). The diffraction efficiency for the $m\ \ th$ order is given by

$$\eta_m = \left[\frac{\sin(m\pi/2)}{m\pi/2}\right]^2, \tag{1}$$

resulting in substantial light loss and multiple ghost images that severely limit practical applications.

Despite these limitations, zone plates established the fundamental principles of diffractive optics and demonstrated the possibility of achieving optical focusing without traditional refractive elements. Their planar geometry and wavelength-dependent focusing properties laid the groundwork for all subsequent diffractive lens developments.

2.2. Fresnel lenses: continuous phase modulation

Fresnel lenses represent a significant advancement by replacing the binary amplitude modulation of zone plates with continuous phase modulation. The lens surface consists of concentric annular prisms that manipulate the optical path length to achieve constructive interference at the focal point, as shown in Figure 1(b). The phase relationship is described by

$$\varphi(r, \lambda) = \frac{2\pi}{\lambda}[n(\lambda) - 1]h(r), \tag{2}$$

where λ is the wavelength, $h(r)$ represents the height profile and $n(\lambda)$ is the wavelength-dependent refractive index. The height profile at a particular wavelength λ_0 follows

$$h(r) = \frac{\lambda_0}{2\pi[n(\lambda_0) - 1]}(\varphi \bmod 2\pi), \tag{3}$$

where mod means modulus, creating a characteristic sawtooth pattern with periodic phase resets.

The key innovation of Fresnel lenses lies in their ability to achieve theoretically 100% diffraction efficiency at the design wavelength λ_0 by eliminating the opaque regions present in zone plates which can be seen in Figure 1(g). The diffraction efficiency of the $m\ \ th$ order of such Fresnel lenses at design wavelength λ_0 can be expressed as

$$\eta_m = \left\{\frac{\sin[\pi(m - 1)]}{\pi(m - 1)}\right\}^2. \tag{4}$$

However, Fresnel lenses still suffer from severe chromatic aberration due to the wavelength dependence of the diffraction process. The efficiency rapidly decreases for wavelengths deviating from the design wavelength.

Additionally, the continuous height profile presents significant fabrication challenges, particularly for visible wavelength applications where sub-micrometer features are required.

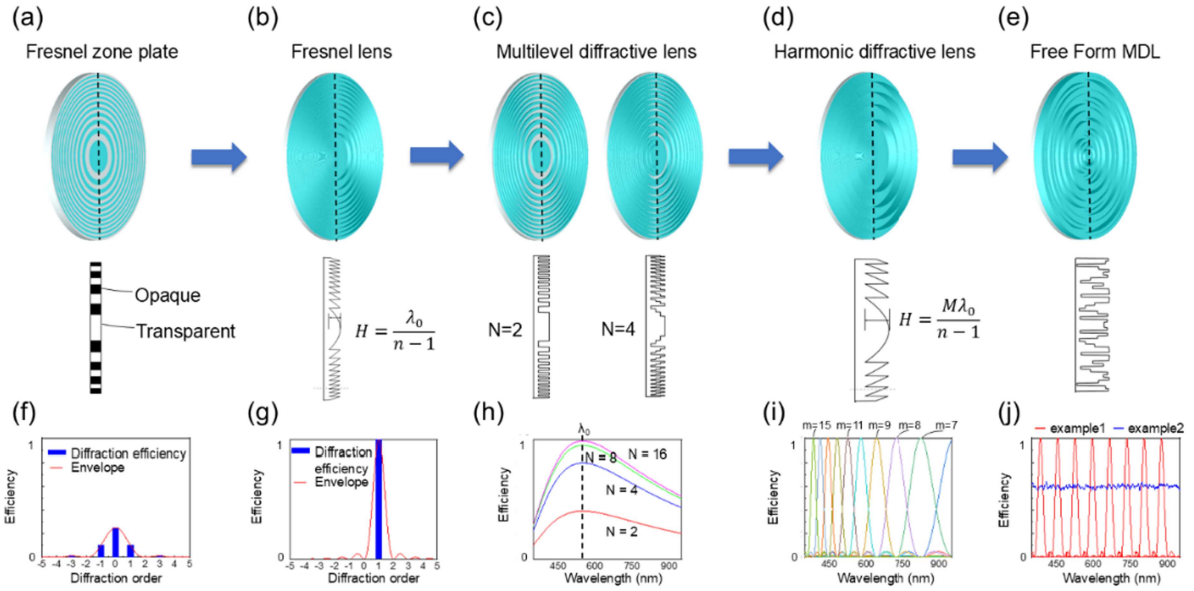

Figure 1. (a)-(e) Evolution of diffractive lens technologies [2]. The upper row shows schematic diagrams of different diffraction lenses, and the lower row shows schematic diagrams of the height distribution on the black dotted lines in the corresponding lenses. H is the height, n is the refractive index, λ_0 is the design wavelength, N is the number of gray-scale levels, M is the harmonic order of the design wavelength λ_0. (f) Diffraction efficiency of Fresnel zone plates at different orders of design wavelength. (g) Diffraction efficiency of Fresnel lenes at different orders of design wavelength. (h) Diffraction efficiency of a multilevel diffractive lens with respect to wavelengths and different gray-scale levels. The black dashed line indicates the design wavelength λ_0. (i) Diffraction efficiency of a harmonic diffractive lens with respect to wavelengths and different diffractive orders, where m is diffractive order. (j) Diffraction efficiency of two free-form MDLs, example1 for the MDL operating at equally spaced discrete wavelengths and example 2 for the MDL operating at broadband spectra.

2.3. Multilevel diffractive lenses: discrete approximation strategy

The emergence of binary optics in the 1980s introduces MDLs as a practical solution to the fabrication challenges of continuous Fresnel profiles. MDLs approximate the continuous phase profile using discrete height levels, typically 2^N levels achievable through N sequential binary lithography and etching steps as shown in Figure 1(c).

The diffraction efficiency of MDL at the mth order with Nlevels is given by

$$\eta_m^N = \left\{ \frac{\sin[\pi(1-m)]}{\pi(1-m)} \right\}^2 \left[\frac{\sin(\pi/N)}{\pi/N} \right]^2, \tag{5}$$

reaching over 95% at the design wavelength for 8-level structures ($N \geq 8$) as shown in Figure 1(h). This discrete approximation strategy enables precise fabrication using established semiconductor processing techniques while maintaining high optical efficiency. The multilevel approach also provides better control over higher-order diffraction, concentrating most of the diffracted light into the desired first order.

Despite their fabrication advantages and high efficiency at the design wavelength, conventional MDLs still exhibit significant chromatic aberration. The efficiency degradation with wavelength follows the same fundamental relationship as Fresnel lenses, limiting their application in broadband optical systems. The regular, analytically-derived height distribution constrains the design space and prevents optimization for achromatic performance.

2.4. Harmonic diffractive lenses: multi-wavelength optimization

Harmonic diffractive lenses, proposed in 1995, represent the first systematic attempt to address chromatic aberration in diffractive optics. The harmonic diffractive lens is designed such that the optical path length

transition between adjacent facets is an integer multiple M of the design wavelength λ_0, which means the total thickness of this lens is $H = M\lambda_0/(n-1)$ as shown in Figure 1(d). The diffraction efficiency of m th order for a harmonic diffractive lens is given by

$$\eta_m = \left\{ \frac{\sin\{\pi[M\alpha(\lambda) - m]\}}{\pi[M\alpha(\lambda) - m]} \right\}^2, \tag{6}$$

where α is the detuning parameter, defined as $\alpha = \lambda_0[n(\lambda) - 1]/\lambda[n(\lambda_0) - 1]$. This approach enables high efficiency at m th harmonic wavelengths $\lambda_m = M\lambda_0[n(\lambda) - 1]/m[n(\lambda_0) - 1]$, where each harmonic achieves 100% efficiency at its corresponding diffraction order as shown in Figure 1(i).

The harmonic approach successfully demonstrates that diffractive lenses can achieve high efficiency at multiple discrete wavelengths while maintaining the same focal length. As the harmonic number M increases, more wavelengths achieve high efficiency, improving the average performance across a broader bandwidth. This technology has found practical applications in specialized scenarios such as micro-objectives for specific laser wavelengths.

However, harmonic lenses suffer from two fundamental limitations. First, the harmonic wavelengths are fixed according to the design parameters, lacking the flexibility in wavelength selection for specific applications. Second, the efficiency drops significantly at intermediate wavelengths between harmonics, resulting in poor performance for broadband illumination. These constraints motivated the search for more flexible design approaches.

2.5. Free-form AMDLs: inverse design revolution

To further increase the degrees of freedom in design, a new class of diffractive lenses, denoted free-form MDLs, has been proposed in recent years. The height profile of the free-form AMDL is irregular and quite different from that of conventional diffractive lenses, as shown in Figure 1(e). Unlike zone plates, Fresnel lenses, and harmonic diffractive lenses that rely on predetermined analytical phase profiles, free-form AMDLs abandon these mathematical constraints entirely.

Free-form AMDLs can realize many more functionalities, such as discrete multi-wavelength operation with arbitrary wavelength spacing [example 1 in Figure 1(j)] or broadband achromatism [example 2 in Figure 1(j)]. The free-form MDL is designed by inverse design as introduced in Section 3. By setting different figures of merit [47–50], AMDLs with various functionalities can be realized—whether targeting broadband achromatism, extended depth of focus, or large field of view applications.

3. AMDL design methodologies and inverse optimization

The development of AMDLs represents a fundamental paradigm shift from traditional analytical design approaches to sophisticated computational optimization methodologies. This transformation leverages inverse design principles to discover optimal height distributions that achieve unprecedented achromatic performance across broad wavelength ranges.

3.1. Inverse design framework: from performance to structure

Traditional diffractive lens design relies on predetermined analytical phase profiles, such as parabolic or hyperbolic distributions derived from geometric optics. These approaches impose fundamental limitations by fixing the phase profile and leaving limited degrees of freedom for optimization. Inverse design represents a revolutionary departure by starting with desired performance characteristics and computationally discovering the optimal optical structure to achieve these goals.

The core philosophy treats each design element—the height of each annular zone in AMDLs—as an independent optimization variable, dramatically expanding the design space. This target-driven methodology enables simultaneous optimization of multiple objectives, such as achieving high efficiency across

broad wavelength ranges while maintaining excellent imaging quality and manufacturability. The resulting height profiles often exhibit irregular, non-intuitive patterns that deliver superior performance compared to conventional analytical designs.

The AMDL optimization problem can be expressed as maximizing an objective function F subject to discrete height constraints:

$$\max F(h(r)) \;\; subject \;\; to \;\; h(r) \in \left\{0, \frac{H}{N}, \frac{2H}{N}, \ldots, H\right\}, \tag{7}$$

where $h(r)$ represents the height distribution, H is the maximum height, and N is the number of discrete levels. The objective function must capture essential performance requirements, with common formulations including focal intensity maximization

$$F_1 = \frac{1}{N_\lambda} \sum_{N_\lambda} I_0(\lambda), \tag{8}$$

where N_λ is the number of wavelengths optimized in achromatic design, I_0 denotes the intensity at focus, and power concentration optimization

$$F_2 = \frac{1}{N_\lambda} \sum_{N_\lambda} \frac{\int_0^{1.5w} I(r, \lambda) r dr}{\int_0^{w} I(r, \lambda) r dr}, \tag{9}$$

where w is the full width at half maximum (FWHM) and $I(r, \lambda)$ is the light intensity distribution on focus plane.

3.2. Optimization algorithms for AMDL design

The AMDL design space represents an extremely complex optimization landscape with M^N possible configurations for Nzones and M height levels. A typical design with 100 zones and 8 levels yields approximately 8^{100} combinations, creating a highly multimodal landscape with numerous local optima. The design of AMDLs requires sophisticated optimization algorithms capable of handling discrete design variables while navigating complex, multi-modal objective landscapes. Unlike conventional diffractive elements with analytical solutions, AMDLs rely entirely on computational optimization to discover optimal height distributions across multiple zones.

Direct Binary Search (DBS) [51,52] has emerged as the most widely used algorithm for AMDLs design due to its effectiveness with discrete optimization problems. DBS systematically perturbs each zone by evaluating all possible height values while keeping other zones fixed, updating the height if improvement is achieved. The algorithm guarantees convergence to a local optimum and naturally handles discrete constraints without requiring continuous relaxation. The algorithmic flow involves: (1) Initialize height distribution randomly or heuristically; (2) For each zone, evaluate objective function for all possible heights; (3) Update to the height yielding maximum improvement; (4) Repeat until convergence. While DBS offers simplicity and stability, it suffers from susceptibility to local optima and slow convergence for large-scale problems.

Global optimization algorithms address these limitations by maintaining population diversity and exploring multiple regions simultaneously. Genetic algorithms [53,54] provide population-based optimization that maintains diversity through integer encoding of height levels and tournament selection. Crossover operators exchange zone information between parent solutions, with zone-block crossover preserving spatial correlations. Mutation operators introduce new genetic material through random or neighborhood-based height changes. Particle Swarm Optimization (PSO) [55] adapts to discrete design spaces through modified velocity update equations and multi-swarm strategies. Simulated Annealing enables escape from local optima through probabilistic acceptance of inferior solutions, with temperature

schedules controlling the exploration-exploitation balance. These global methods can discover superior solutions compared to DBS but require careful parameter tuning and increased computational resources.

Hybrid optimization strategies combine global search capabilities with local convergence properties. Common approaches use genetic algorithms or particle swarm optimization for global exploration followed by DBS refinement, achieving both global optimality and rapid local convergence [56]. Recent advances include adjoint methods for efficient gradient computation through continuous relaxation, and topology optimization approaches that treat height distribution as a density field [57–62]. These methods enable rapid convergence but may miss discrete solutions not accessible through continuous paths.

4. AMDL design results and advanced fabrication technologies

The rapid development of AMDLs over the past decade has yielded remarkable progress in both design sophistication and manufacturing capabilities. This chapter provides a comprehensive review of AMDL demonstrations from 2016 to 2025, organized by technological approaches that integrate design innovations with the enabling fabrication methods. Rather than artificially separating design results from manufacturing technologies, we examine how different fabrication capabilities have driven distinct technological pathways, each with unique advantages and applications.

4.1. Traditional lithographic AMDL technology route

Traditional lithographic techniques—notably electron-beam lithography (EBL) and grayscale lithography (GSL)—underpin the fabrication of early and high-precision AMDLs. EBL enables sub−10 nm resolution by directly writing binary patterns onto electron-sensitive resist, making it ideal for fine-featured diffractive elements such as Fresnel zone plates. However, its high cost, and incompatibility with efficient multilevel structuring—requiring multiple lithography cycles—limit its practicality for complex or large-area lenses. In contrast, GSL overcomes these constraints by spatially modulating exposure dose to generate height-varying resist profiles in a single step, enabling smooth, multilevel topographies essential for broadband achromatic performance positioning it as the dominant enabler of practical AMDLs.

4.1.1. Early breakthrough period (2016–2018)

The field of AMDLs was inaugurated by Wang et al. [41] in 2016 with the first experimental demonstration of a 1D AMDLs capable of broadband operation across the visible spectrum. This pioneering work focused light to a line (akin to conventional cylindrical lenses) and achieved super-achromatic performance over the continuous visible band from 450 nm to 700 nm, as shown in Figure 2(a). The AMDL was fabricated using SC1827 photoresist with a length of 7.5 mm and total thickness of 2.6 μm, representing a significant reduction in thickness compared to conventional refractive achromatic systems. While this first demonstration had a relatively low numerical aperture of 0.013, it successfully validated the inverse design approach for achieving broadband achromatic performance with an overall focus efficiency of approximately 10%. The focusing efficiency, is defined as the ratio of optical power within three times Full Width at Half Maximum (FWHM) of point spread function (PSF) over the whole incident optical power [63].

In the same year, Peng et al. [64] demonstrated a complementary approach by equalizing the spectral focusing performance within the visible spectrum from 410 nm to 690 nm as shown in Figure 2(b). Their silica-based AMDL featured an 8 mm diameter, 1.195 μm thickness, and numerical aperture of 0.04. Importantly, this work included direct performance comparisons with conventional Fresnel lenses, demonstrating that while the AMDL performed slightly worse at the design wavelength (550 nm), its overall performance under broadband illumination was superior, clearly validating the achromatic advantage.

The progression continued in 2018 when Mohammad et al. [65] achieved a significant breakthrough in compact design with an AMDL having 370 μm diameter while reaching a numerical aperture of 0.18, as shown in Figure 2(c). This represented a dramatic size reduction while simultaneously improving the overall efficiency to 22.1%. The same group also demonstrated a simple imaging system composed of two

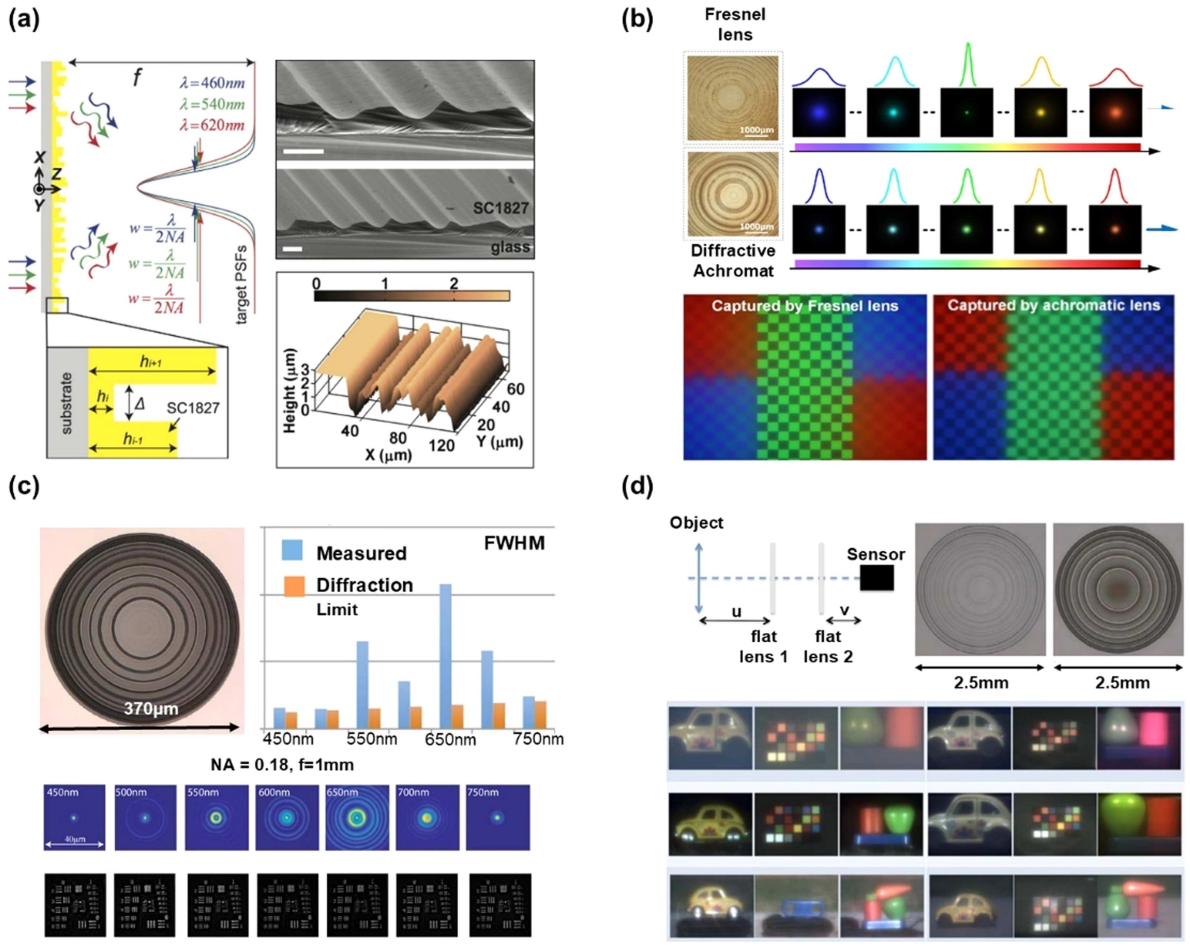

Figure 2. AMDLs in early breakthrough period. (a) 1D broadband AMDL working in the visible region [41]. The insets show schematic illustration of the 1D AMDL, scanning electron microscopy (SEM) image of the fabricated sample, corresponding height profile. (b) Broadband AMDL over the visible range from 410 nm to 690 nm with NA 0.04 and diameter equal to 8 mm [64]. The insets show optical micrograph of the AMDL, results of the focusing performance test and imaging test. (c) Broadband AMDL working in the visible region with NA 0.18 and diameter equal to 370 μm [65]. The insets show microscopy image of the AMDL; full width at half maximum (FWHM) measurement of the focal spot, cross-sectional intensity profile of the focal spot, imaging test. (d) An imaging system composed of two AMDLs [66]. The insets show schematic of the imaging setup, microscopic view of the AMDL, and captured experimental image.

AMDLs [66], showing the potential for multi-element achromatic systems based entirely on diffractive components as shown in Figure 2(d).

4.1.2. Performance enhancement period (2019–2021)

The period from 2019 to 2021 witnessed substantial improvements in both spectral bandwidth and numerical aperture capabilities through refined lithographic processes and optimized design methodologies. Meem et al. in 2020 [67] demonstrated an AMDL with extended spectral coverage from 450 nm to 1000 nm, encompassing both visible and near-infrared regions as shown in Figure 3(a). This lens featured a 3.145 mm diameter, 2.6 μm thickness, and numerical aperture of 0.3, while achieving a focus efficiency of 12%. The extension into the near-infrared presented additional challenges due to increased material dispersion effects, requiring more sophisticated optimization strategies and improved fabrication precision.

A parallel development by Doskolovich et al. in 2020 [68] introduced spectral diffractive lenses (SDLs) capable of focusing multiple prescribed wavelengths to a fixed position, representing a significant advancement over harmonic diffractive lenses with their arbitrary wavelength selection capability as shown in Figure 3(b). Their method employed a non-iterative design approach based on minimizing

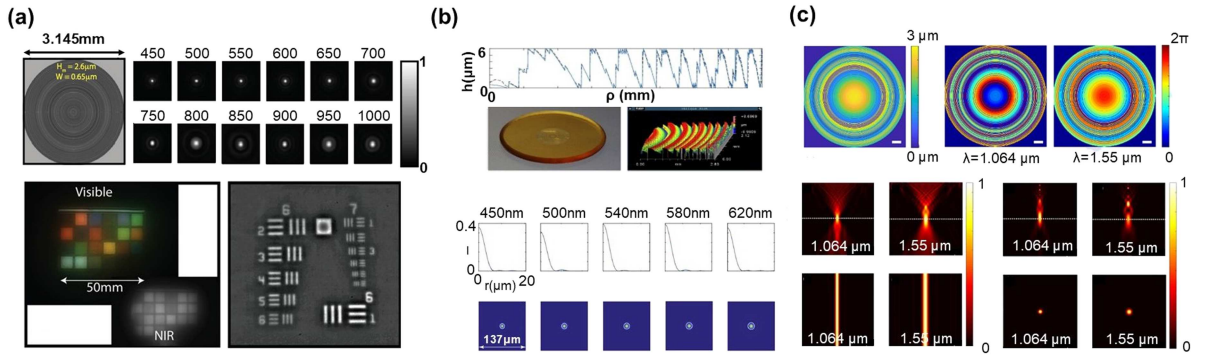

Figure 3. AMDLs in performance enhancement period. (a) Broadband AMDL over the visible and near-infrared range from 450 nm to 1000 nm with NA 0.3 and diameter equal to 3.145 mm [67]. The insets show schematic of the AMDL, measured point spread function (PSF) under broadband illumination; off-axis PSF; modulation transfer function (MTF) characterization, and imaging results. (b) Multiwavelength AMDL working over 450 nm to 620 nm [68]. The insets show height profile of the AMDL, optical micrograph, and intensity profile of focal spot. (c) Dual-wavelength MDLs for near-infrared imaging at 1.064 μm and 1.55 μm wavelengths [69]. The insets show designed height profiles, phase profiles at different wavelengths, simulated intensity profile of focal spot.

the deviation of complex transmission functions at operating wavelengths from individually optimized diffractive lenses. The demonstrated SDL operated at five discrete wavelengths across 450–620 nm with an 8 mm diameter, 6 μm thickness, and numerical aperture of 0.04. Simulation results showed remarkable efficiency of 39.6%, while experimental validation using direct laser writing achieved 16.4% efficiency. The significant simulation-experiment difference highlighted manufacturing precision challenges but confirmed the viability of arbitrary multi-wavelength lens design without the wavelength constraints of harmonic approaches.

Yang et al. in 2021 [69] demonstrated dual-wavelength MDLs specifically designed for near-infrared imaging at 1.064 μm and 1.55 μm wavelengths, common fiber laser frequencies with significant applications in biological and medical imaging as shown in Figure 3(c). The designed PMMA-based lenses featured 280 μm aperture, 10 mm focal length, and multilevel height profiles optimized using a modified direct binary search algorithm that maintained radial symmetry while supporting extension from 1D to 2D designs. Simulation results demonstrated exceptional performance with focusing efficiencies of 72% and 79% for 2D lenses, and 92% and 92% for 1D lenses at 1.064 μm and 1.55 μm respectively. The simulated FWHM values closely approached diffraction-limited performance at 23.19 μm and 29.99 μm for the respective wavelengths.

4.1.3. Special wavelength extensions

The success of visible-spectrum AMDLs motivated exploration of longer wavelengths, where the relaxed fabrication tolerances could potentially enable larger-scale manufacturing. Meem et al. in 2019 [70] demonstrated a polymer AMDL operating in the long-wave infrared region from 8 μm to 12 μm, corresponding to an important atmospheric transmission window for thermal imaging applications as shown in Figure 4(a). This infrared AMDL featured a 15.2 mm diameter and only 10 μm thickness, achieving an experimental average focus efficiency of 43% across the 8–12 μm range despite 25% absorption losses in the polymer material. The lens demonstrated superior imaging quality with 35° field of view and angular resolution less than 0.013°, characterized using two different commercial LWIR image sensors. Significantly, the lens exhibited aberrations comparable to or better than conventional refractive lenses, demonstrating that the achromatic advantages of AMDLs extend beyond simple efficiency considerations to include superior imaging quality. The use of polymer materials enabled manufacturing via imprint lithography, offering dramatic cost reductions and weight savings of over 100 times compared to conventional germanium or silicon-based LWIR optics.

A remarkable extension of AMDL capabilities was demonstrated by Meem et al. in 2021 [71], who achieved unprecedented spectral coverage spanning from visible to long-wave infrared wavelengths (450 nm to 15 μm) using a single diffractive surface as shown in Figure 4(b). This extremely wide

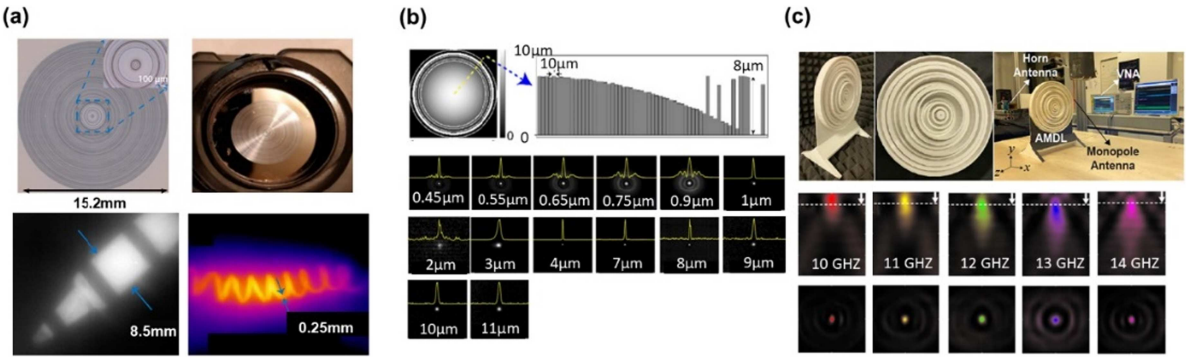

Figure 4. AMDLs for special wavelength extensions. (a) Broadband AMDL over the long-wave infrared region (8–12 μm) with NA 0.45 and diameter equal to 15.2 mm [70]. The insets show microscopy image of the ADML, photograph of the AMDL, and experimental imaging results. (b) AMDL with spectral coverage spanning from visible to long-wave infrared wavelengths (450 nm to 15 μm) [71]. The insets show height profile of the AMDL, intensity profile of focal spot. (c) Broadband AMDL over the microwave region (10–14 GHz) with NA 0.99 and diameter equal to 186 mm [72]. The insets show photograph of the fabricated AMDL and measured intensity profile of focal spot.

bandwidth represents over an order of magnitude larger operating range than any previously demonstrated flat lens. The fabricated AMDL featured a compact 0.992 mm diameter with only 10 μm maximum thickness and 18 mm focal length, maintaining constant focusing performance across the entire spectral range. The lens was fabricated using grayscale lithography in AZ9260 photoresist with 8 μm minimum feature width and up to 100 discrete height levels. Due to substrate transparency limitations, identical lens profiles were fabricated on glass substrates for visible-to-near-infrared operation and silicon substrates for infrared operation. Experimental characterization confirmed excellent achromatic performance with measured Strehl ratios averaging 0.74 across all wavelengths.

The scalability of AMDL concepts to microwave frequencies was demonstrated by Yildırım et al. in 2021 [72] with an ultra-high numerical aperture design (NA ≈ 0.99) operating from 10 GHz to 14 GHz as shown in Figure 4(c). This work incorporated a multi-objective differential evolution algorithm combined with three-dimensional finite-difference time-domain (FDTD) simulations to optimize both the heights and widths of each concentric ring. Uniquely, the focal distance was treated as an optimization parameter rather than a predetermined constraint, eliminating the need for fixed center frequency and providing an alternative approach to phase profile engineering. The resulting microwave AMDL had a diameter of 186 mm and thickness of 26 mm, achieving FWHM values less than 0.554λ and focusing efficiencies varying between 28% and 45.5%. The lens was fabricated using 3D printing with PLA material and experimentally validated, with numerical and experimental results showing excellent agreement. The design was also scaled to visible wavelengths (380–620 nm) to demonstrate achromatic focusing behavior.

4.1.4. Large-scale AMDL breakthrough

Xiao et al. in 2022 [56] achieved a landmark breakthrough in large-scale AMDL fabrication, demonstrating the first centimeter-scale achromatic flat lens through advanced grayscale laser lithography as shown in Figure 5. Five polymer lenses with diameters ranging from 1 mm to 10 mm and uniform thickness of 15 μm were successfully fabricated using 405 nm grayscale laser lithography in AZ4562 photoresist on glass substrates. The lenses operating across an ultra-broad bandwidth from 400 nm to 1100 nm cover the entire visible to near-infrared spectrum. The fabrication process achieved remarkable precision with average manufacturing errors less than 150 nm (<1% relative error), enabling near-diffraction-limited performance. Experimental characterization confirmed exceptional achromatic performance with measured Strehl ratios exceeding 0.8 and focusing efficiencies approaching theoretical limits. Comparative white-light imaging experiments demonstrated superior performance compared to conventional refractive lenses, marking a significant milestone toward practical large-scale flat optics applications and establishing grayscale lithography as a viable route for centimeter-scale AMDL manufacturing.

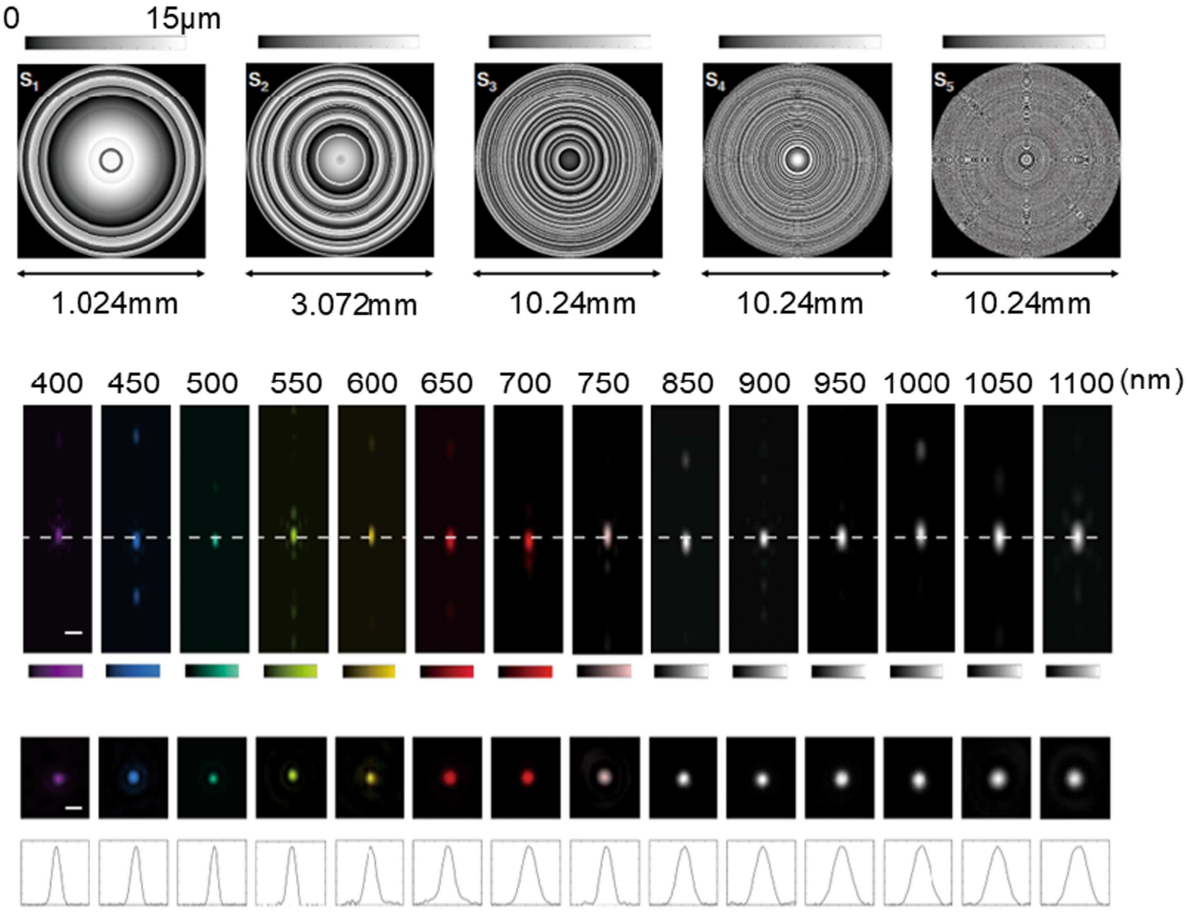

Figure 5. Large-scale AMDLs working from 400 nm to 1100 nm covering the entire visible to near-infrared spectrum [56]. The insets show the schematic height profiles of the five fabricated samples, measured intensity profile of focal spot.

4.2. Emerging manufacturing-driven technology routes

The limitations of traditional lithographic approaches in terms of throughput, cost, and design flexibility have motivated the development of alternative manufacturing technologies that enable new AMDL design paradigms. These emerging approaches leverage additive manufacturing, direct laser writing, and novel material platforms to achieve capabilities beyond those accessible through conventional fabrication methods.

4.2.1. 3D printing and additive manufacturing AMDLs

Additive manufacturing enables maskless, direct fabrication of multilevel diffractive structures through layer-by-layer material deposition or photopolymerization. Fused deposition modeling (FDM) extrudes thermoplastic filament through a heated nozzle, building structures with moderate vertical resolution—suitable for applications where feature sizes exceed hundreds of micrometers, such as in long-wavelength regimes. In contrast, two-photon polymerization (TPP) leverages nonlinear absorption of focused femtosecond laser pulses within photosensitive resin to induce localized polymerization, achieving sub-micron resolution and true 3D freeform capability. While FDM offers cost efficiency and compatibility with large-area fabrication, it is limited by surface roughness and relatively coarse feature control. TPP delivers high precision and complex multilevel geometries in a single step but suffers from low throughput and scalability constraints due to its serial writing nature. Together, these methods provide flexible, application-adaptive pathways for diffractive optics beyond conventional lithography.

Pan et al. in 2023 [73] made an important progress in high-numerical aperture achromatic metalenses through 3D-printed multilayer structures as shown in Figure 6(a), overcoming fundamental trade-offs

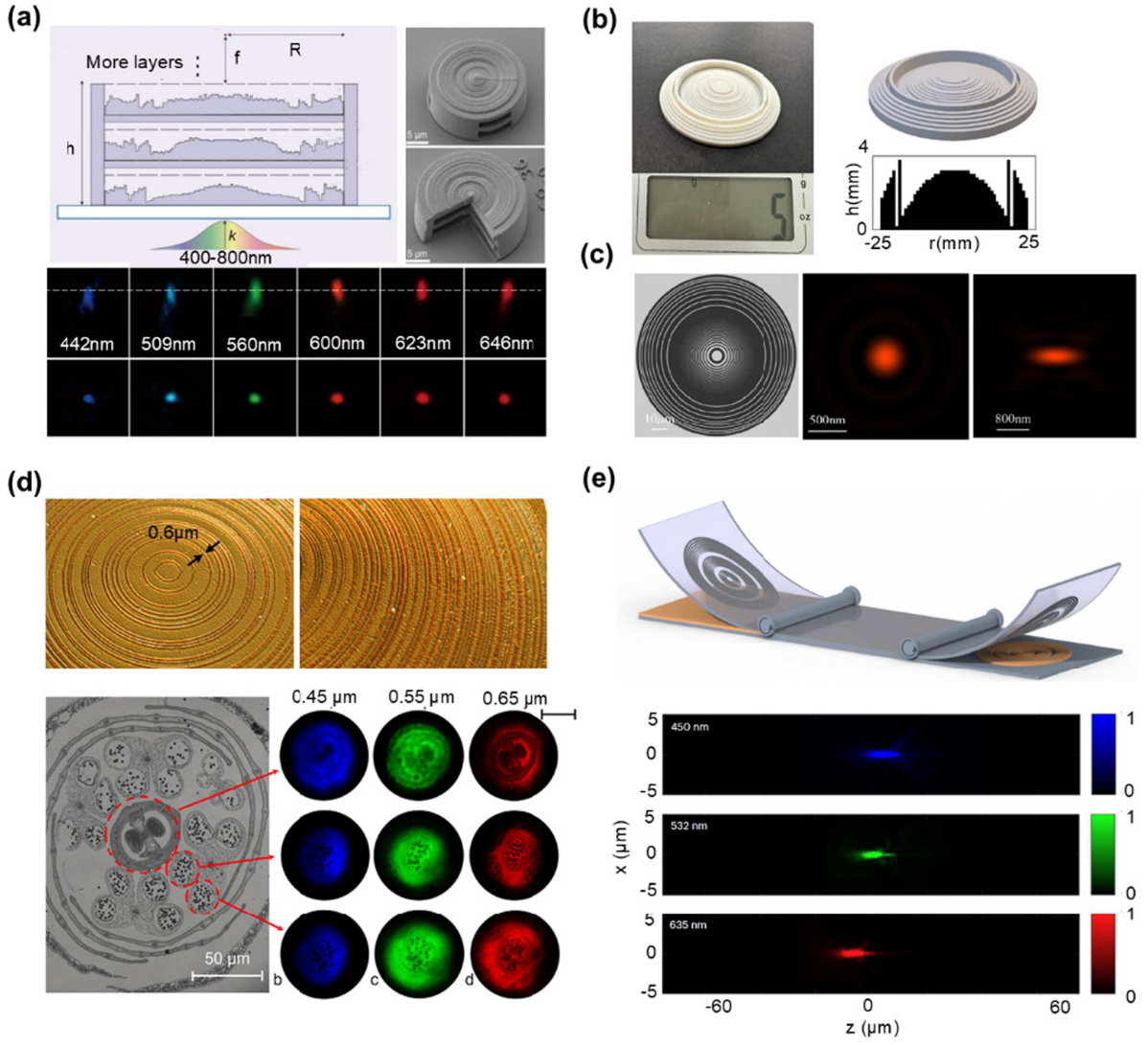

Figure 6. Emerging manufacturing-driven AMDLs. (a) 3D-printed multilayer structures achromatic diffractive lens [73]. The insets show schematic of the multilayer structure, SEM image of the fabricated lens, intensity profile of focal spot. (b) 3D printing terahertz MDLs [55]. The insets show optical photograph of the AMDL, the height profile. (c) Graphene oxide achromatic lens operating at three visible wavelengths (450 nm, 550 nm, 650 nm) [75]. The insets show design schematic of the AMDL, intensity profile of focal spot. (d) Multi-wavelength achromatic graphene lenses operating at 0.45, 0.55, and 0.65 μm wavelengths [76]. The insets show microscopy image of the AMDL and imaging results. (e) A 1 cm diameter RGB achromatic lens with high numerical aperture working at 450, 532, and 633 nm wavelengths [77]. The insets show fabrication process illustration and measured intensity profile of focal spot.

between bandwidth and NA in single-layer designs. The key innovation employed topology optimization with adjoint method to inversely design multilayer achromatic diffractive lenses fabricated using two-photon polymerization lithography (TPL) in low-refractive index IP-Dip resin ($n \approx 1.5$). This approach leverages the superior Abbe number (~35.2) of polymeric materials—a dimensionless measure of material dispersion, where higher values indicate lower chromatic aberration [74]—compared to high-index materials like Si (5.5) or TiO_2 (9.86), significantly reducing material dispersion.

The optimized three-layer design with 1.6 μm spacing achieved unprecedented performance: 20 μm diameter lenses operating across 400–800 nm bandwidth with NA = 0.5 and 0.7, demonstrating average focusing efficiencies of 42% and 20% respectively. The TPL fabrication process enabled one-step lithographic patterning of complex multilayer structures with 200 nm minimum feature resolution, eliminating alignment challenges of traditional multi-step processes. Proximity-effect compensation techniques included 500 ms intervals between adjacent ring exposures and sequential printing from center to edge.

Experimental validation confirmed excellent broadband imaging performance under white light and RGB illumination.

Shi et al. in 2023 [55] demonstrated the application of 3D printing technology for fabricating terahertz MDLs as shown in Figure 6(b), addressing manufacturing challenges in the THz frequency range (0.11–0.17 THz). The key innovation combined inverse design methodology using particle swarm optimization and differential evolution algorithms with additive manufacturing, utilizing polylactic acid (PLA) material with refractive index ~1.57 and achieving 0.2 mm height resolution. The computational approach employed cylindrical coordinate FDTD simulations combined with Rayleigh-Sommerfeld diffraction theory to enable efficient simulation of large-scale structures.

Three lens types were demonstrated: communication system lenses (100 mm focal length), high numerical aperture lenses (NA = 0.89), and achromatic lenses operating across the WR–6.5 band. The optimized 21-level lens achieved near zero bit error rates in THz communication systems, comparable to conventional Teflon lenses while offering significant advantages in weight, size, and cost-effectiveness. Experimental validation confirmed excellent agreement with simulations, demonstrating successful focusing performance and achromatic behavior across the target frequency range.

4.2.2. Laser direct writing and novel material platforms

In micro- and nanoscale fabrication, Laser Direct Writing (LDW) has emerged as a widely adopted technique for patterning optical surfaces with high precision. It employs a tightly focused, ultrafast laser beam—typically operating in the picosecond to femtosecond pulse regime—to selectively remove material through localized ablation, enabling the direct inscription of features with resolutions ranging from the sub-micron down to the nanometer scale. This approach facilitates the production of complex, high-resolution micro-nano structures tailored to a specific design, making them ideal for fabrication of multilayer structures.

Li et al. in 2024 [75] introduced a revolutionary fabrication approach for ultrathin flat lenses using designer graphene oxide (GO) films as shown in Figure 6(c), achieving extraordinary focusing properties through simultaneous phase and amplitude modulation. The key innovation employed a one-step direct laser writing method to create concentric rings of reduced graphene oxide (rGO), where laser parameters precisely control ring width, thickness, transmission, and refractive index. This approach represents a significant manufacturing breakthrough, eliminating complex multi-step lithographic processes typical of traditional flat lens fabrication.

The design methodology combined Rayleigh-Sommerfeld diffraction theory with genetic algorithm optimization to determine optimal ring numbers and radii. Two lens types were demonstrated: a sub-diffraction lens achieving FWHM of ~0.506λ and an achromatic lens operating at three visible wavelengths (450 nm, 550 nm, 650 nm) with focal lengths of 246.4 μm, 246.2 μm, and 246.8 μm respectively. The achromatic lens maintained consistent focusing performance across the visible spectrum with FWHM values of 0.267 μm, 0.301 μm, and 0.305 μm at the respective wavelengths.

Cao et al. in 2025 [76] introduced multi-wavelength achromatic graphene diffractive lenses as shown in Figure 6(d) representing a breakthrough in single-material ultrathin flat lens design. The key innovation employed a partial intensity resonance (PIR) mechanism based on Rayleigh-Sommerfeld diffraction theory, eliminating the need for iterative algorithms and enabling millimeter-scale lens design in microseconds. This approach leverages graphene's dispersionless nature across ultraviolet to terahertz frequencies, addressing fundamental material bandgap limitations that have prevented single-material broadband achromatic lenses.

Two high numerical aperture AMDLs were demonstrated: a visible RGB lens (NA = 0.71) operating at 0.45, 0.55, and 0.65 μm wavelengths, and a near-infrared communication band lens (NA = 0.65) covering 0.850, 1.33, and 1.55 μm. The fabrication process utilized one-step laser nanoprinting on graphene oxide films, creating submicron concentric rings through photochemical reduction. Experimental validation showed exceptional accuracy with focal length deviations less than 0.15% from designed values and theoretical-experimental FWHM differences under 10.6%.

4.2.3. Large-scale manufacturing technologies

Large-scale manufacturing of diffractive optics relies on replication-based techniques such as nanoimprint lithography (NIL), which enable high-throughput, low-cost patterning over wafer- to panel-scale areas.

NIL operates by mechanically embossing a rigid or flexible master template into a UV-curable polymer layer coated on a substrate; subsequent UV exposure solidifies the pattern, which is then demolded to yield a faithful replica of the nanostructure. Limitations include dependency on high-fidelity master templates, potential defect propagation over large areas, and restricted aspect ratios due to demolding constraints. These techniques represent the most viable pathway for transitioning lab-scale diffractive designs into commercially scalable products.

Choi et al. in 2025 [77] reported a remarkable manufacturing achievement for large-aperture achromatic lenses through roll-to-plate (R2P) printing technology as shown in Figure 6(e). The key innovation employed topological inverse design with full FDTD simulations across ~10,000λ areas, enabling fabrication of a 1 cm diameter RGB achromatic lens with high numerical aperture (0.7) using low-index nanoimprint resin ($n \approx 1.5$). This approach overcomes scalability limitations of previous designs requiring high-index materials like TiO_2 or GaN.

The R2P manufacturing process enables mass production compatibility with 90 nm minimum feature resolution and low aspect ratios suitable for industrial fabrication. Axisymmetric structures and Green's function transformation reduced computational complexity from cubic to linear scaling. Experimental validation confirmed excellent RGB performance at 450, 532, and 633 nm wavelengths with successful integration into compact holographic near-eye displays for VR applications.

4.3. Advanced design method-driven innovations

The evolution of AMDL technology has been significantly accelerated by the development of design methodology that enable the exploration of complex optimization landscapes and the discovery of non-intuitive solutions. These advanced approaches combine multiple optimization strategies and leverage computational advances to achieve unprecedented performance levels.

4.3.1. Topology optimization and multilayer design

The development of topology optimization approaches has enabled the design of complex multilayer AMDL structures that achieve performance levels impossible with single-layer designs. Pan et al. [73] exemplifies this approach, where topology optimization with adjoint methods enabled the inverse design of three-layer structures that overcome fundamental bandwidth-NA trade-offs. The methodology treats the height distribution as a continuous density field, enabling gradient-based optimization while maintaining manufacturability constraints.

4.3.2. Hybrid optimization frameworks

Zu et al. in 2025 [78] introduced a fast and efficient hybrid inverse design framework for multifunctional diffractive lenses, combining shape-constrained topology optimization (SCTO) with discrete particle swarm optimization (DPSO) to achieve cross-dimensional cooperative optimization. The key innovation addresses fundamental limitations of traditional unit-cell approaches and pure topology optimization by providing abundant design degrees of freedom while maintaining fabrication-friendly features.

The framework employs concentric ring structures to ensure polarization insensitivity and structural robustness while utilizing 2D axisymmetric simulations to drastically reduce computational complexity. Two immersed silicon carbide diffractive lenses were demonstrated with near-unity numerical apertures. The extended depth-of-focus diffractive lens achieved a DOF over four times the wavelength with 23% maximum diffraction efficiency, approaching theoretical limits. The broadband achromatic lens as shown in Figure 7 suppressed chromatic aberrations across 300 nm bandwidth (850–1150 nm) with ultra-high NA of 0.984 and 10% average efficiency.

Fabrication utilized focused ion-beam milling with 30 kV acceleration voltage, creating structures with 4 height levels (0.2–0.5 μm) and 50 nm radial resolution. The global optimization solver enhanced figure-of-merit by 37.6% over local optimization alone, demonstrating the critical importance of hybrid approaches that combine the strengths of different optimization methodologies.

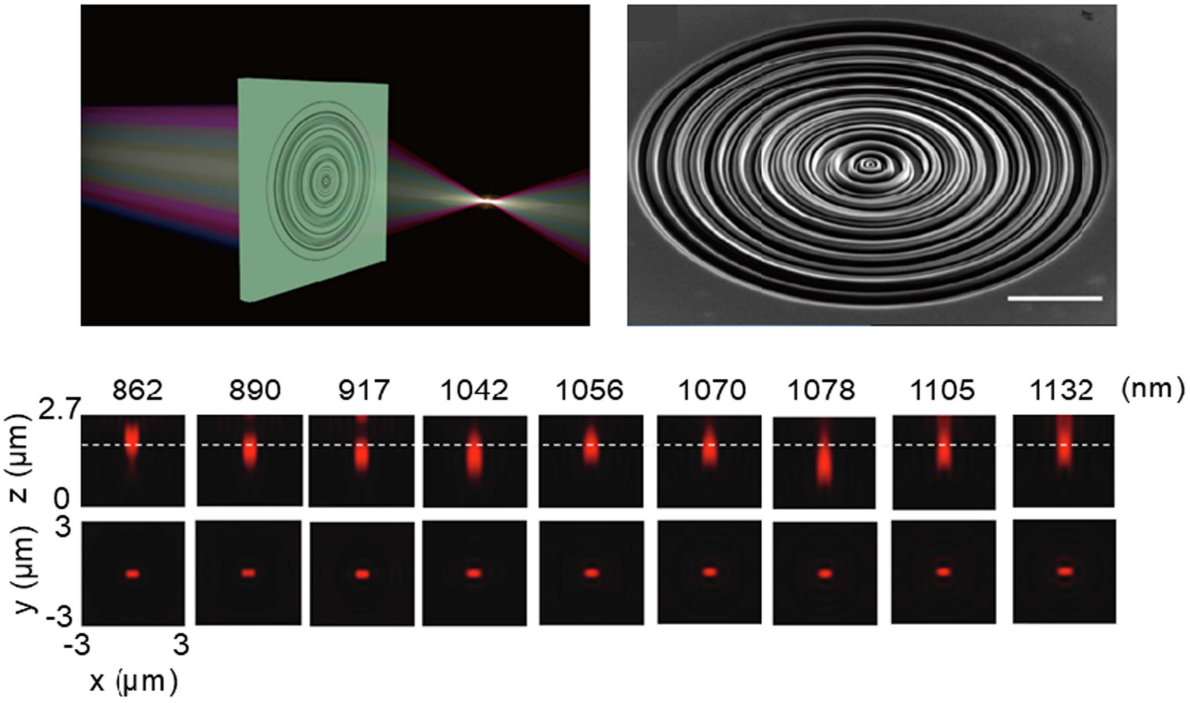

Figure 7. The broadband achromatic lens working across 300 nm bandwidth (850–1150 nm) with ultra-high NA of 0.984 and 10% average efficiency [78]. The insets show schematic of the AMDL, SEM image, measured intensity profile of focal spot.

4.3.3. Inverse design and computational advances

The development of efficient computational methods has been crucial for enabling the design of large-scale AMDL structures. Choi et al. [77] demonstrated how axisymmetric assumptions and Green's function transformations can reduce computational complexity from cubic to linear scaling, enabling full-wave simulations of centimeter-scale structures. Similarly, Cao et al. proposed PIR mechanism [76] that eliminates the need for iterative optimization, enabling rapid design of complex achromatic structures.

These computational advances have democratized AMDL design by reducing the computational resources required for optimization, enabling broader exploration of the design space and faster iteration cycles. The integration of machine learning approaches, as detailed in Chapter 6, represents the next frontier in this computational evolution.

The diverse technological pathways for AMDLs, from traditional lithography to emerging manufacturing techniques, have been extensively explored in this chapter. To provide a clear overview and facilitate comparison of the key achievements, Table 1 summarizes the performance metrics and characteristics of the representative works discussed herein, categorized by their primary fabrication technology route. Furthermore, to visually contextualize the rapid evolution of this field, Figure 8 presents a timeline of major fabrication breakthroughs over the past decade.

5. Performance boundaries and comparative analysis

5.1. Physical constraints and performance bounds of AMDLs

The practical implementation of AMDLs faces fundamental physical constraints that limit their achievable performance. Understanding these limitations is crucial for realistic design expectations and optimization strategies. This section analyzes the theoretical performance bounds based on light frequency-domain coherence theory and examines the fundamental trade-offs between key design parameters.

Traditional analysis of achromatic flat lenses assumes ideal phase profiles following the hyperbolic relation

Table 1. Comparison of representative AMDLs.

References	Year	NA	Diameter	Wavelength (Frequency)	Efficiency	Design method	Fabrication technique
[41]	2016	0.013	7.5 mm	450–700 nm	~10%	Direct Binary Search	Grayscale lithography
[64]	2016	0.04	8 mm	410–690 nm	-	Particle Swarm Optimization	Photolithography, Reactive ion etching
[65]	2018	0.18	370 μm	450–750 nm	22.1%	Direct Binary Search	Grayscale lithography
[70]	2019	0.371	15.2 mm	8–12 μm	43%	Gradient Descent Assisted Binary Search	Grayscale lithography
[67]	2020	0.3	3.145 mm	450–1000 nm	12%	Gradient Descent Assisted Binary Search	Grayscale lithography
[68]	2020	0.04	8 mm	450–620 nm	16.4%	Brute-Force Search	Laser direct writing
[69]	2021	0.028	280 μm	1.064 μm 1.55 μm	72%(Sim.) 79%(Sim.)	Direct Binary Search	-
[71]	2021	0.027	0.992 mm	0.45–11μm	-	Direct Binary Search	Grayscale lithography
[72]	2021	~0.99	18.6 cm	10–14 GHZ	~35%	Multi-objective Differential Evolution	3D-printing
[56]	2022	0.1	10 mm,	400–1100 nm	31%	Gradient Descent Assisted Binary Search	Grayscale lithography
[73]	2023	0.5	20 μm	400–800 nm	44.2%	Topology Optimization	Two-photon polymerization lithography
[55]	2023	~0.89	40 mm	0.11–0.17 THZ	-	Particle Swarm Optimization Differential Evolution Gradient Descent	3D-printing
[75]	2024	0.37	200 μm	450,550,650 nm	-	Genetic Algorithm	Laser direct writing
[76]	2025	0.71	500 μm	450,550,650 nm	-	Partial intensity resonance	Laser direct writing
[77]	2025	0.7	10 mm	450,532,633 nm	10%	Topology Optimization	Nanoimprint
[78]	2025	0.984	26μm	850–1150 nm	13.6%	Topology Optimization, Particle Swarm Optimization	Focused ion beam milling

Table note: NA = Numerical Aperture; Sim. = Simulated value. Efficiency values denote average focusing efficiency across the operating band unless specified otherwise. "-" indicates that the specific value was not explicitly stated in the referenced work.

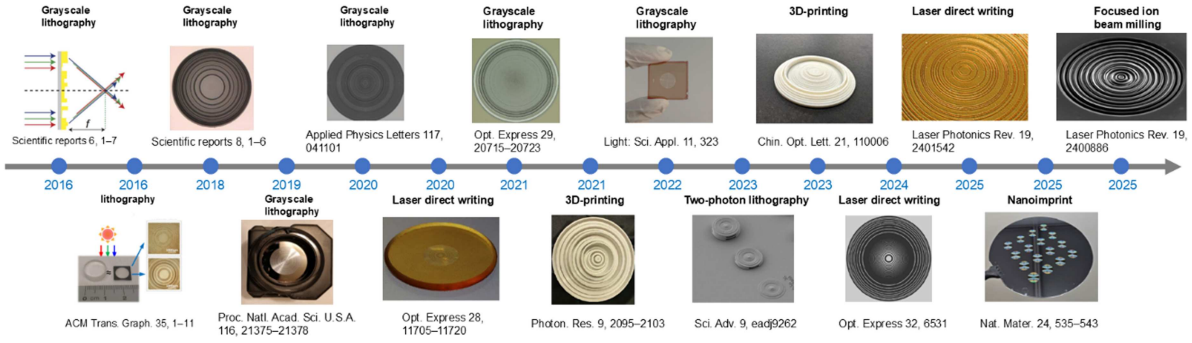

Figure 8. Timeline of key milestones in the fabrication of AMDLs.

$$\Phi(\rho, \omega) = -\frac{\omega}{c}(\sqrt{\rho^2 + F^2} - F), \tag{10}$$

where ω, F, ρ, and c represent angular frequency, focal length, radial coordinate, and speed of light, respectively. However, practical AMDLs exhibit phase distortions $\Delta\Phi(\rho, \omega)$ that deviate from this ideal profile, making conventional group delay analysis inadequate.

Xiao et al. [56] introduced a frequency-domain coherence framework to address this limitation. The frequency domain mutual coherence function between two coordinates ρ_1 and ρ_2 on the exit pupil is defined as:

$$J_\omega(\rho_1, \rho_2) = \left\langle e^{i\Delta\Phi(\rho_1,\omega)} e^{-i\Delta(\rho_2,\omega)} \right\rangle_\omega, \tag{11}$$

where $\langle\rangle_\omega$ denotes frequency averaging. The real part of J_ω indicates the degree of coherence: + 1 represents perfect constructive interference, while −1 indicates complete destructive interference between sub-waves from ρ_1 and ρ_2 as shown in Figure 9(a).

The normalized coherence function at focus $J_\omega(F)$ relates directly to focusing performance through:

$$J_\omega(F) = \frac{F^2}{\pi^2 R^4} \iint_\Sigma J_\omega(\rho_1, \rho_2) \frac{1}{r_1 r_2} d\Sigma_1 d\Sigma_2, \tag{12}$$

where R is the lens radius and r_i represents the distance from ρ_i to focus.

The upper bound of focusing efficiency is constrained by:

$$\max J_\omega(F) \approx \max \frac{\langle Eff \rangle_\omega}{w_{max}^2}, \tag{13}$$

where Eff is the focus efficiency (ratio of optical power within 3 × FWHM of the PSF to total transmitted power) and w_{max} is the maximum normalized PSF diameter across the spectrum.

For AMDLs, the phase profile follows $\varphi_{AMDL}(\rho, \omega) = (\omega/c)[n(\omega) - 1]h(\rho)$, where $h(\rho)$ and $n(\omega)$ represent the height distribution and refractive index, respectively. The coherence degradation directly translates to efficiency reduction, establishing a quantitative link between design parameters and performance limitations.

Xiao et al. systematically analyzed the coherence distribution for AMDLs with varying parameters as shown in Figure 9(b). For a fixed NA (0.1), working spectrum (400–1100 nm), and material (AZ4562), the maximum coherence max $\mathrm{Re}J_\omega(\rho_1, \rho_2)$ exhibits clear dependencies on diameter and thickness. Smaller,

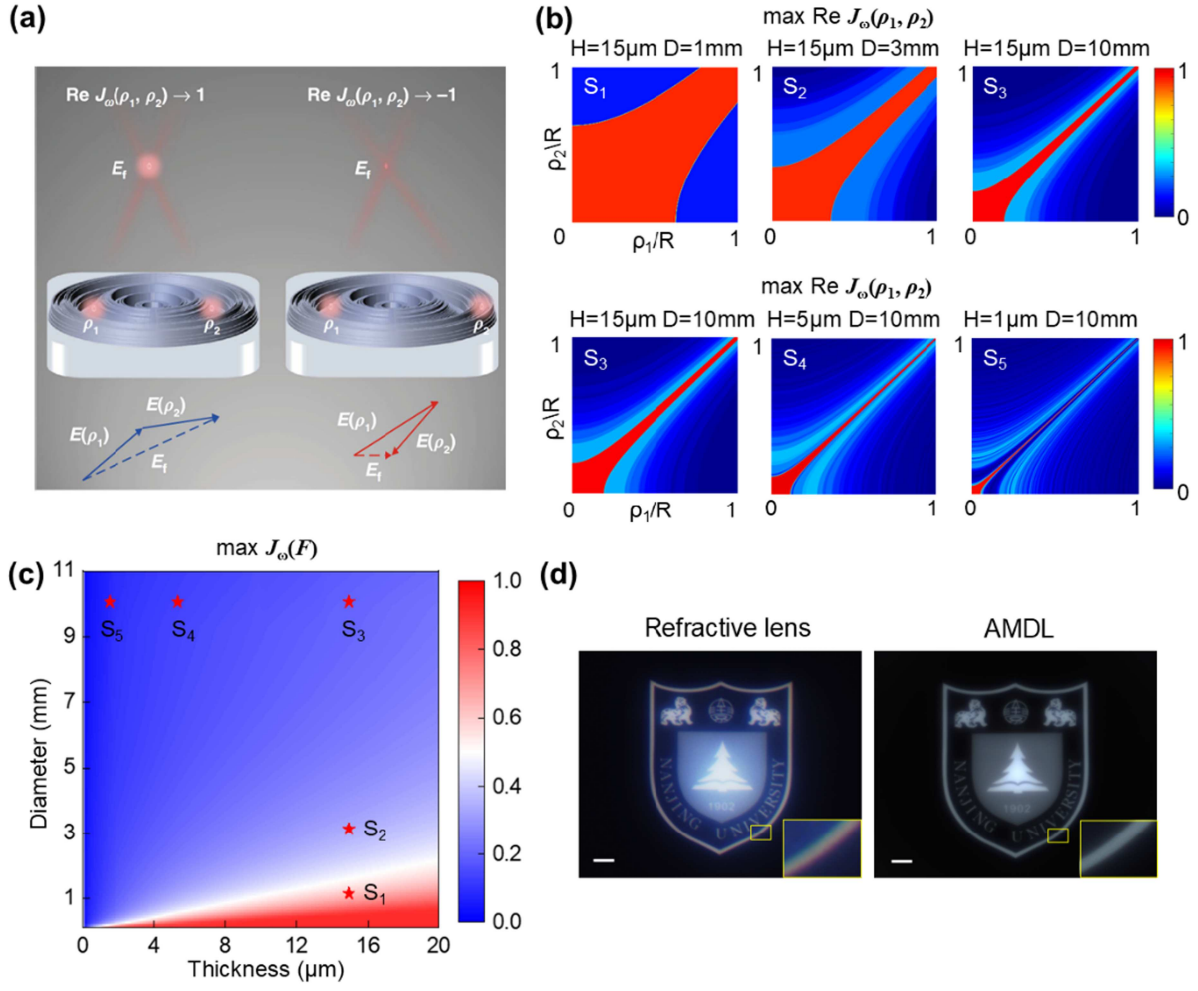

Figure 9. Fundamental physical constraints of AMDLs [56]. (a) Schematics of the coherence of wave distortion in MDL. (b) The distribution of max $J_\omega(\rho_1, \rho_2)$ with thickness fixed at 15 μm and diameter equal to 1, 3, 10 mm, respectively; the distribution of max $J\omega(\rho_1, \rho_2)$ with diameter fixed at 10 mm and thickness equal to 15, 5, 1 μm, respectively. (c) The max $J_\omega(F)$ with respect to different samples in dimensions of diameter and thickness. (d) Image of Nanjing University logo taken from sample S_3 and a refractive lens.

thicker lenses maintain high coherence regions across larger areas in (ρ_1, ρ_2) space, while larger or thinner lenses show progressively degraded coherence as shown in Figure 9(c).

The fundamental restriction relation can be approximated as:

$$D_{max} \approx \frac{4(n_{max} - 1)H}{(1 - \sqrt{1 - \max J_\omega(F)})NA}, \tag{14}$$

where n_{max} is the maximum refractive index over the spectrum. This relationship reveals that diameter scaling requires proportional thickness increases to maintain focusing performance, establishing a fundamental trade-off for large-scale AMDL design.

A comprehensive performance index $P = D(1 - \sqrt{1 - J_\omega(F)})NA$ incorporates size, numerical aperture, and focus performance simultaneously. Comparison of reported AMDLs and achromatic metalenses reveals that AMDLs achieve order-of-magnitude higher comprehensive performance due to their larger achievable thickness. The effective thickness $H_{eff} = (n_{max} - 1)H$ emerges as a critical parameter determining overall performance limits.

Experimental validation using five AMDL samples (S1-S5) with diameters from 1–10 mm and thicknesses from 1–15 μm confirmed theoretical predictions. The measured max $J_\omega(F)$ values of 0.72, 0.43, 0.21, 0.11, and 0.03 for samples S1-S5 respectively demonstrate the strong correlation between coherence theory and experimental performance. They also evaluated the imaging performance of the AMDL by comparing it with a conventional refractive lens (LE1234), as shown in Figures 9(d).

The working bandwidth $\Delta\lambda$ significantly influences the restriction relations, though analytical expressions remain complex due to approximations in the derivation. Numerical simulations indicate that focus performance improves as working bandwidth decreases for fixed diameter, thickness, and NA. Material dispersion characteristics also play crucial roles, with higher refractive index materials offering advantages within the constraint framework.

This analysis establishes that while AMDLs face inherent physical constraints, understanding these limitations through frequency-domain coherence theory enables rational design approaches that approach theoretical upper bounds of its performance. The framework provides quantitative tools for balancing competing requirements and identifying optimal design spaces for specific applications.

5.2. Comparative analysis: AMDLs versus achromatic metalenses

As two prominent technological pathways within the field of flat optics, achromatic metalenses and thickness-modulated MDLs offer distinct approaches to overcoming chromatic aberration in ultra-thin optical systems. Their underlying physical mechanisms, design philosophies, and fabrication paradigms differ significantly, leading to distinct advantages and limitations. Both platforms also show considerable potential for large-scale manufacturing [8–10,79], making them promising for industrial applications. Understanding these differences is essential for selecting the appropriate platform for a given application—whether it prioritizes spectral bandwidth, optical efficiency, numerical aperture, aperture size, functional versatility, or manufacturability.

5.2.1. Phase modulation mechanism and design flexibility

The fundamental difference between metalenses and MDLs lies in their phase modulation mechanisms—and, consequently, in their design methodologies and computational frameworks.

Metalenses achieve phase control through the interaction of light with subwavelength structures of fixed height, commonly referred to as meta-atoms. Phase modulation is then achieved entirely by varying the in-plane geometry: the shape, dimensions, orientation, or lattice arrangement of each meta-atom. The optical response of each meta-atom is predominantly obtained through full-wave electromagnetic simulations, as their behavior is governed by complex near-field interactions, Mie resonances, or geometric (Pancharatnam-Berry) phase effects that lie beyond the scope of scalar approximations. This lateral

parameter space is extraordinarily rich granting metalenses unparalleled freedom in wavefront engineering.

In contrast, thickness-modulated MDLs operate primarily in the height (axial) dimension. The lateral footprint of each diffractive zone—typically ring-shaped due to rotational symmetry—remains geometrically uniform within a given zone. Phase control is achieved by varying the physical height profile h(r) of the transparent material. The phase shift is governed by the scalar relation:

$$\phi = \frac{2\pi}{\lambda}(n(\lambda) - 1)h(r), \tag{15}$$

where λ is the wavelength, n is refractive index. The response intrinsically wavelength-dependent but also highly predictable and amenable to rapid computation via scalar diffraction theory or Fourier optics methods. While full-wave simulations can still be employed for high-precision validation—especially in cases of deep etching or high index contrast—the majority of MDL designs are optimized using scalar-based inverse design or iterative algorithms, drastically reducing computational overhead and enabling large-aperture, broadband optimization in practical timeframes.

5.2.2. Feature size and thickness

Metalenses are characterized by sub-wavelength features, typically ranging from tens to hundreds of nanometers, depending on the operating wavelength. These small feature sizes enable precise control over the wavefront but impose stringent fabrication requirements. Single-layer metalenses are usually very thin, which makes them particularly suitable for compact and lightweight applications.

On the other hand, MDLs utilize larger feature sizes, typically in the micrometer range, allowing for more relaxed fabrication tolerances. The thickness of MDLs is also greater, depending on the required phase modulation depth and aperture size. This makes MDLs compatible with established micro-optical fabrication techniques such as grayscale photolithography, diamond turning, and additive manufacturing. But what determines the manufacturing challenge is often the aspect-ratio (height to width) of the structures.

5.2.3. Functional versatility

One of the key advantages of metalenses is their functional versatility. Their local phase control allows for simultaneous manipulation of amplitude, phase, and polarization, enabling functionalities such as polarization beam splitting, orbital angular momentum generation, and dynamic focusing with tunable materials. This makes them ideal for integrated photonic circuits, compact sensors, and augmented reality systems.

MDLs, governed by scalar diffraction, are typically polarization-insensitive and functionally focused on focusing or imaging. While they can achieve some level of multifunctionality through hybrid designs or cascaded architectures, their flexibility is generally lower compared to metalenses.

5.2.4. Polarization selectivity

Another advantage of metalenses is their native support for polarization-dependent phase control. By utilizing geometric phase or other mechanisms, metalenses can achieve flexible polarization multiplexing, enabling applications such as chiral optics and vector beam generation. This capability is particularly valuable for polarization-sensitive applications in fields like quantum optics and telecommunications.

MDLs, on the other hand, are typically polarization-insensitive, as their phase modulation is based on the optical path length and does not inherently depend on polarization. While polarization functionality can be added through hybrid integration, it adds complexity and may reduce overall system performance.

5.2.5. Chromatic correction mechanisms

Achieving achromatic performance remains a key challenge for both platforms, with strategies shaped by their distinct physical architectures. Metalenses exploit multiple dispersion control mechanisms.

Dispersion-engineered meta-atoms, designed via modulating both phase and group delay, enable broadband achromatic focusing across continuous wavelength bands. Spatial multiplexing—transverse or longitudinal—corrects discrete wavelengths by assigning dedicated meta-atom groups, albeit at the cost of fill factor or increased thickness. Metalenses can also adopt inverse design frameworks akin to MDLs, optimizing meta-atom arrangements to balance bandwidth, efficiency, and other metrics. In contrast, MDLs rely primarily on scalar inverse design: their height profiles are optimized under rotational symmetry to maximize constructive interference across broad spectral ranges, enabling efficient large-aperture broadband operation.

6. Machine learning-enhanced AMDLs design

The integration of AI, particularly deep learning, into optical system design is redefining the development of high-performance imaging devices. In the context of AMDLs—thin, lightweight alternatives to traditional refractive optics—AI has emerged as a transformative enabler, allowing for substantial improvements in chromatic correction, manufacturability, and overall imaging performance.

Recent progress in computational optics and nanophotonic imaging has demonstrated the potential of flat optics to overcome traditional trade-offs between aperture size, bandwidth, and thickness [80–93]. Their findings underscore a broader paradigm shift towards data-driven co-design of optical elements and image reconstruction algorithms. This evolution has laid the groundwork for a deeper convergence between AMDL technologies and machine learning methodologies, enabling a new generation of intelligent, high-performance optical systems. In the following sections, we examine how this convergence manifests across various design philosophies, highlighting representative advances and their implications for future development.

6.1. Post-processing correction with deep learning

Early applications of deep learning to AMDL-associated imaging systems largely adopted a modular strategy, in which the diffractive lens was predesigned and fabricated using conventional methods, while neural networks were applied subsequently to correct for chromatic aberration and other degradations in captured images. This approach treated the optical and computational components as separate entities, allowing researchers to retrofit intelligence onto physically constrained optics.

Among these initial efforts, a notable study [94] employed a Convolutional Neural Network (CNN) to enhance the achromatic imaging quality of a system based on a singlet AMDL as shown in Figure 10(a). The key was a training strategy that bridged the simulation-to-reality gap by combining simulated datasets with experimentally measured Point Spread Functions (PSFs). This hybrid approach allowed effective aberration correction and significantly improved image quality, demonstrating the feasibility of compact high-performance imaging with a single flat lens.

Building upon such foundational work, another solution was later presented [95] that employed a deep-learning model to overcome the inherent chromatic aberrations of imaging systems based on flat lenses as shown in Figure 10(b). This approach is significant as it computationally corrects for both transverse and axial chromatic aberrations simultaneously, without requiring prior estimation of the PSF. This data-driven post-processing technique enabled the production of high-quality color images from a simplified optical setup, demonstrating a path toward reducing the size, cost, and weight of imaging systems.

Hybrid optical systems [96] leveraging computational correction have continued to show promising advances. For instance, a refractive/diffractive duplex lens custom-optimized to eliminate chromatic aberration at key wavelengths and mitigate off-axis distortions was developed as shown in Figure 10(c). Residual artifacts were then corrected with a UNet trained on noise-augmented lab data, achieving robust performance across varying conditions. By combining custom-fabricated optics with adaptive reconstruction, such systems deliver image quality comparable to multi-lens assemblies.

Recent studies have further extended post-processing strategies to metalenses. One work [89] demonstrated that deep learning can refocus RGB channels and correct vignetting in single metalens imaging, as

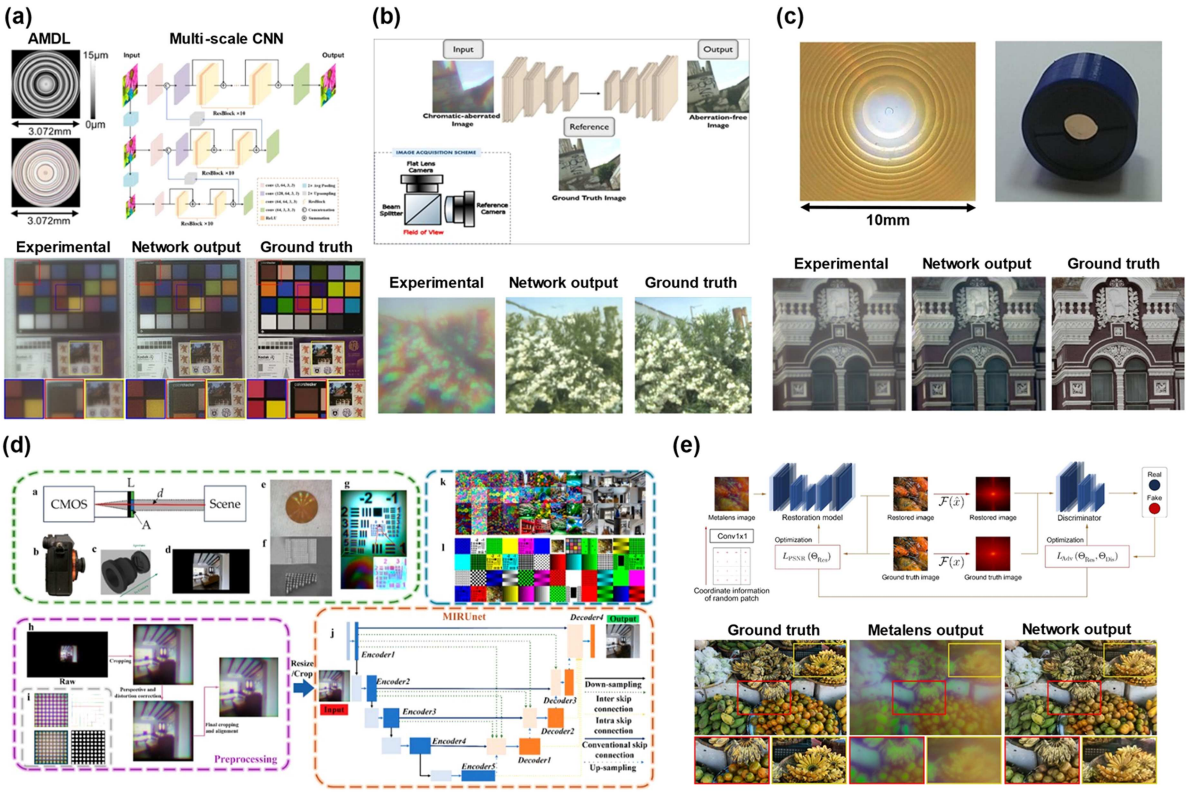

Figure 10. Post-Processing Correction with Deep Learning. (a) Profiles and photographs of the fabricated AMDL, the deep multi-scale CNN for image restoration, and representative experimental results of the AMDL imaging system compared with commercial cell phone cameras. [94]. (b) Data-driven chromatic aberration correction using real-scene training on visible-spectrum flat lens imaging [95]. (c) Hybrid refractive–diffractive lens with neural network restoration, showing the fabricated ring-shaped structure, 3D-printed component, and artifact-free imaging results. [96]. (d) Overview of metalens imaging and reconstruction. Shown are the optical path and system configuration, fabricated devices and their nanostructures, representative raw imaging results and preprocessing workflow, as well as the MIRUnet framework and corresponding training and calibration datasets for image restoration [89]. (e) Deep-learning-driven end-to-end metalens imaging, showing network architecture and representative restoration results compared to raw captures [81].

shown in Figure 10(d), thereby restoring full-color image quality without hardware modification. Another study proposed an end-to-end framework integrating broadband metalenses with a restoration network [81], as shown in Figure 10(e), enabling aberration-free, high-resolution imaging comparable to ground truth.

6.2. End-to-end co-design of AMDLs and neural networks

End-to-end co-design relies on constructing physical models of AMDLs in a differentiable and computationally efficient form, enabling gradients from downstream tasks to propagate jointly through both the optical and computational domains. In practice, scalar diffraction theory, like Fresnel or angular spectrum propagation, can be reformulated into differentiable operators [90], while the AMDL surface is discretized into phase-delay levels expressed as complex exponentials, making the lens geometry directly trainable. To accelerate computation and handle complex multi-parameter responses across wavelengths and polarizations, neural networks have been employed as surrogate forward models that map nanostructure geometries to full-parameter Jones matrices [82]. This approach enables fast, differentiable, and fabrication-aware optimization of large-scale metasurfaces, allowing system-level loss functions—such as image fidelity or task-specific metrics—to drive the co-optimization of both the optical layout and the reconstruction network, ultimately enhancing overall system performance.

A compelling example of this [97] integrated approach is provided by a lithography-aware co-design method for diffractive optical elements (DOEs). This framework discretizes the AMDL height profile into a finite number of fabrication-friendly levels and jointly optimizes these with a gated Wiener–Lucy deconvolution network as shown in Figure 11(a). This method not only accounts for process-induced height deviations but also enhances robustness and image quality under real-world manufacturing constraints.

Early efforts in optical-neural co-design laid a solid foundation for integrating diffractive optics with neural reconstruction algorithms. For instance, a joint optimization framework [98] for DOE phase profiles and U-Net-based reconstruction networks was developed, employing MSE-SSIM loss functions to mitigate aberrations in integral imaging systems as shown in Figure 11(b). Rotationally symmetric diffractive achromats combined with ResUNet architectures [99] were also proposed as shown in Figure 11(c), achieving full-spectrum imaging across wide fields of view through energy-regularized optimization. Optical-neural co-design for SPAD-based super-resolution imaging [100] was implemented to overcome sensor resolution limits via single-shot phase mask coding without mechanical scanning as shown in Figure 11(d). In addition, an end-to-end optimization framework integrating AMDLs with reconstruction algorithms [101] demonstrated enhanced resolution and extended depth of field as shown in Figure 11(e).

Building upon these advances, a more recent study [102] proposed a hybrid design scheme for large-aperture diffractive apertures (DAs) as shown in Figure 11(f). This method first employs a Wiener filter for initial optimization, followed by fine-tuning with a ResUnet. The approach significantly reduces memory requirements and facilitates large-aperture optimization, achieving superior imaging performance compared to traditional end-to-end methods. Crucially, the findings emphasize that joint optimization of the DA and downstream algorithms is essential for reliable high-performance imaging, as optimizing solely for focusing efficiency is insufficient. It was also identified that DAs with higher maximum height, larger F-number, and smaller aperture tend to deliver better imaging quality.

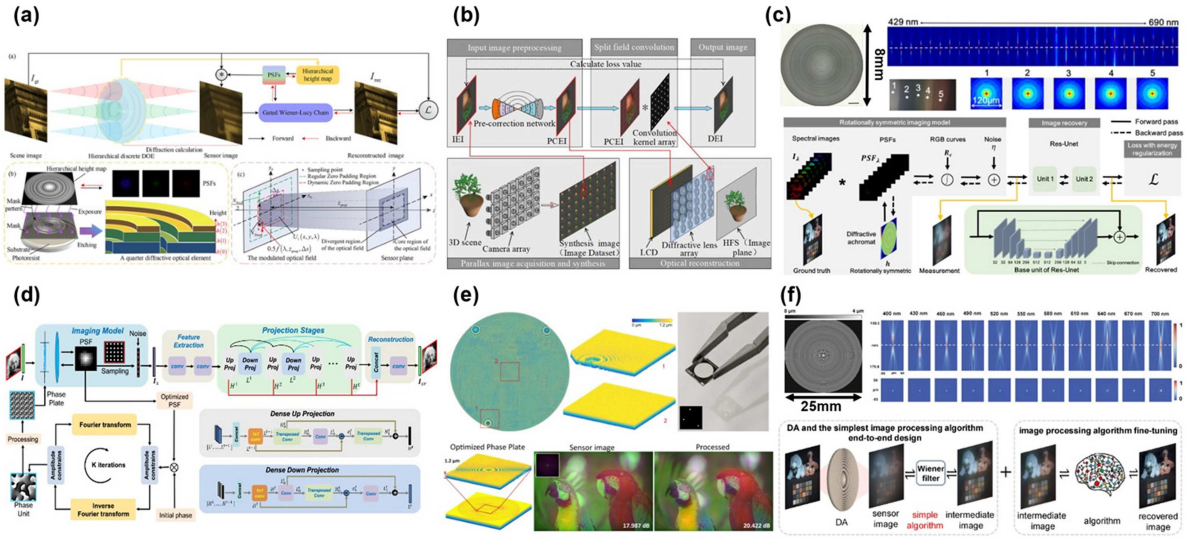

Figure 11. End-to-End Co-Design of AMDLs and Neural Networks. (a) Illustration of the end-to-end diffractive imaging system lithography adaptation design, including the hierarchical-dynamic simulation framework, the hierarchical discrete DOE lithography adaptation scheme, and the padding regions for different zero-padding strategies used in diffraction calculations. [97]. (b) Workflow of the proposed end-to-end optimization for integral imaging with a DOE, showing the process from parallax image acquisition and synthesis, through joint optimization of the DOE and aberration correction, to the final optical reconstruction. [98] (c) End-to-end learning framework for diffractive achromat (DA) design and image recovery, with simulated performance of Fresnel and DA lenses (axial intensity profiles, PSFs, OTFs) and a microscopy image of the fabricated DA. [99]. (d) Joint learning framework of the imaging model and reconstruction network. The PSF for the SPAD array is optimized and converted to a phase mask, and the reconstruction network iteratively restores images through back-projection stages. [100]. (e) Optimized DOE for imaging, including a DOE for super resolution with interleaved lens regions and caustic, and a single element optimized for 25 mm focusing with corresponding PSF and deconvolved images. [101]. (f) Hybrid design scheme for large-aperture diffractive apertures [102].

These studies illustrate that co-designed AMDL systems can significantly outperform conventional designs in both imaging quality and working efficiency. By embracing AI as a native component of optical system design rather than as a downstream corrective tool, these methods unlock new levels of integration and adaptability.

6.3. Function-oriented inverse design with machine learning

Machine learning has demonstrated significant value not only in general-purpose imaging but also in the specialized inverse design of AMDLs. This approach focuses on creating lens structures tailored to specific optical goals.

For example, two distinct machine learning-assisted design frameworks for advanced diffractive optics have been demonstrated [103,104]. In an earlier study [103], supervised learning was employed to accelerate the optimization of polarization-insensitive bidirectional lenses as shown in Figure 12(a), with two-photon 3D printing enabling efficient prototyping while bypassing computational bottlenecks in full-wave simulations. Building on the general paradigm of machine learning-enabled design, a subsequent work [104] implemented an inverse design strategy to realize wavelength-multiplexed trifocal operation through spectral band-specific focal length tuning and cost-effective gray-scale lithography as shown in Figure 12(b).

Notably, Zhang et al. [105] demonstrated a neural network-driven inverse design approach specifically targeting extended depth-of-field through DOEs as shown in Figure 12(c). Their method employs a wave-optics-informed neural network to inversely design DOE phase profiles that maximize depth-of-field while maintaining high resolution. Unlike conventional DOE optimization that relies solely on physical models, their approach incorporates a differentiable wave propagation layer within the network, enabling end-to-

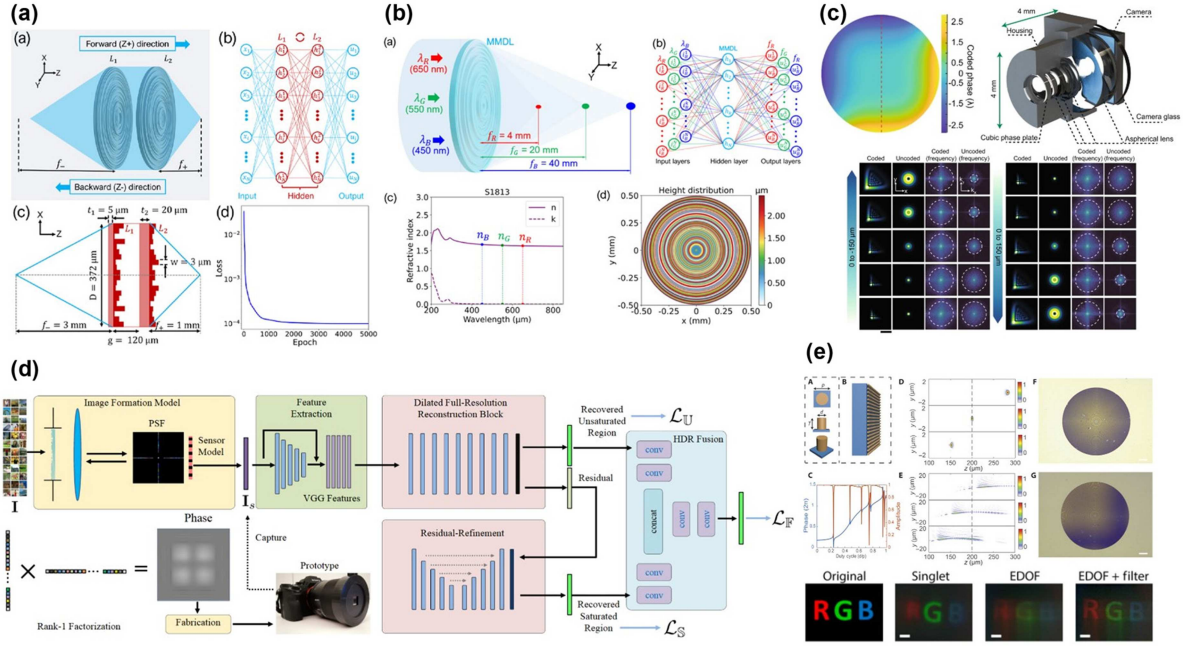

Figure 12. Function-Oriented Inverse Design with Machine Learning. (a) Bidirectional focusing diffractive lens designed via machine-learning-assisted inverse design, enabling different focal lengths for forward and backward propagation. The fabricated device and training convergence are shown. [103]. (b) Schematic of a wavelength-multiplexed multifocal multilevel diffractive lens (MMDL) showing its design, the neural network used for height optimization, the refractive index of the photoresist, and the resulting optimized height profile of the concentric rings. [104]. (c) Modulation phase and surface profile of the DOE in the integrated microscope, spatial and frequency characteristics of the point spread function (PSF) with and without the DOE across different depths, and a 3D rendering of the compact microscope architecture. [105]. (d) Rank−1 DOE used for single-shot HDR imaging, illustrating the light encoding process and CNN-based reconstruction for highlight recovery and fusion [79]. (e) Metalens-enabled full-color computational imaging, depicting the metasurface design and example reconstructed images under white-light illumination [106].

end optimization directly from imaging performance metrics. The network learns to generate phase masks that create depth-invariant PSFs across a 300-μm range, effectively encoding depth information that can be computationally decoded. This methodology achieved a remarkable 10 × increase in depth-of-field without sacrificing resolution, and the network also decodes the resulting complex wavefront, showing how AI-driven inverse design can overcome trade-offs between depth-of-field and resolution.

Beyond these applications, machine learning has been extended to other advanced functionalities. One study [79] introduced a rank−1 parameterization of DOEs for single-shot high-dynamic-range (HDR) imaging as shown in Figure 12(d), encoding saturated highlights into unsaturated regions and reconstructing clipped information via a tailored network, achieving over 7 dB PSNR improvement. Another work [106] combined metasurface optics with computational imaging for full-color imaging as shown in Figure 12(e), using a single NA~0.45 metalens with a spectrally invariant point spread function to enable white-light imaging and digital reconstruction while mitigating chromatic aberrations.

The convergence of machine learning and AMDL design marks a pivotal moment in the evolution of computational optics. Early applications centered on using neural networks for post hoc image restoration have matured into integrated frameworks, where lens geometry and image processing algorithms are co-optimized from the ground up. This co-design ethos, particularly when combined with inverse design methodologies, has proven especially powerful in crafting AMDLs for novel functionalities such as spectral multiplexing and focal tunability. As fabrication-aware simulation tools become more differentiable and surrogate modeling grows more efficient, we anticipate that the training of optical elements and neural modules will occur increasingly within shared, feedback-rich loops. This will pave the way for ultra-compact, multifunctional imaging systems that are not only achromatic and efficient but also tailored for specific tasks through data-driven optimization. In this future, AI will not merely assist in optical design—it will define it.

7. Conclusions and outlook

This review has traced the remarkable evolution of AMDLs from their conceptual origins to current state-of-the-art implementations, highlighting the transformative impact of computational design methodologies, advanced manufacturing techniques, and AI integration. The development of AMDLs represents a fundamental paradigm shift in optical engineering—from analytical design approaches constrained by mathematical formulations to sophisticated inverse optimization strategies that discover optimal solutions within expanded design spaces.

The technological progression documented in this review demonstrates how AMDLs have successfully addressed the persistent challenge of chromatic aberration while maintaining practical manufacturability. Early proof-of-concept demonstrations have evolved into sophisticated implementations spanning diverse spectral ranges, from visible light to terahertz frequencies, with apertures scaling from micrometers to centimeters. This evolution has been enabled by several key technological breakthroughs: (1) inverse design methodologies that optimize free-form height distributions across continuous spectral ranges; (2) advanced fabrication techniques including high-precision lithography, 3D printing, and roll-to-plate processes; and (3) theoretical frameworks such as frequency-domain coherence theory that provide quantitative understanding of fundamental performance limitations.

The categorization of AMDL implementations by manufacturing approach provides valuable insights into the relationship between fabrication techniques and achievable performance. Traditional lithographic methods have demonstrated remarkable progress, culminating in centimeter-scale devices with broadband achromatic performance. Emerging techniques including 3D printing [107], laser direct writing on novel materials like graphene oxide, and roll-to-plate processes are expanding the application space through cost reduction, scalability improvements, and new material platforms. Each manufacturing pathway presents distinct advantages and limitations that must be considered in the context of specific application requirements.

Theoretical analysis based on frequency-domain coherence theory has established quantitative relationships between key design parameters—lens diameter, numerical aperture, spectral bandwidth, and focusing efficiency—revealing fundamental trade-offs that constrain AMDL performance. These insights enable

rational design approaches that approach theoretical performance bounds while balancing competing requirements for specific applications. Furthermore, a comparative analysis between AMDLs and achromatic metalenses has been conducted, elucidating their respective characteristics, advantages, and trade-offs.

More significantly, the integration of AI with AMDL design represents a frontier with extraordinary potential. The progression from post-processing correction to end-to-end co-optimization and function-oriented inverse design demonstrates how machine learning approaches are redefining the development of high-performance optical systems. By embracing AI as a native component of optical system design rather than as a downstream corrective tool, researchers are unlocking new levels of integration and adaptability.

Looking forward, several promising research directions emerge from this review:

1) Advanced Manufacturing Techniques: Further development of high-precision [108–111], large-scale fabrication methods [112,113] will be crucial for transitioning AMDLs from laboratory demonstrations to commercial applications. Particular emphasis should be placed on techniques that enable mass production while maintaining nanometer-scale feature control.
2) Novel Material Platforms: Exploration of new materials with enhanced optical properties, including higher refractive indices, reduced dispersion, and improved environmental stability, could significantly expand the performance envelope of AMDLs.
3) Multifunctional Integration: Future research should explore the integration of AMDLs with additional optical functionalities such as polarization control, wavefront sensing, and dynamic tunability, potentially leading to highly compact multifunctional optical systems.
4) AI-Driven Design Automation: As fabrication-aware simulation tools become more differentiable and surrogate modeling grows more efficient, we anticipate that the training of optical elements and neural modules will occur increasingly within shared, feedback-rich loops, enabling automated design of application-specific optical systems.
5) Theoretical Framework Expansion: Further development of theoretical frameworks that account for non-ideal effects such as fabrication errors, material nonlinearities, and environmental factors will be essential for predicting and optimizing real-world performance.
6) Application-oriented Optimization: Tailoring AMDL designs for specific applications [106,114–119]—from consumer electronics to scientific instrumentation and telecommunications—will require specialized optimization approaches that balance application-specific requirements with manufacturing constraints.

The convergence of computational design methodologies, advanced manufacturing techniques, and AI is enabling a new generation of achromatic flat optics with unprecedented performance characteristics. As these technologies continue to mature, AMDLs are poised to revolutionize optical system design across diverse application domains, offering compelling advantages in terms of size, weight, cost, and functionality. By providing optical engineers with essential technical insights and identifying promising research directions, we hope this review will accelerate innovation in this rapidly advancing field and inspire new approaches to addressing the fundamental challenges of optical system design.

Acknowledgements

Tao Li thanks the support from Dengfeng Project B of Nanjing University.

Disclosure statement

The authors report there are no competing interests to declare.

Funding

This work was supported by the National Natural Science Foundation of China [Grant Nos. 62325504, 62288101, 92250304].

References

[1] Hariharan P. Superachromatic lens combinations. Optics Laser Technology. 1999;31:115–118. doi: 10.1016/S0030-3992(99)00011-0

[2] Li T, Chen C, Xiao X, et al. Revolutionary meta-imaging: from superlens to metalens. Photonics Insights. 2023;2:R01. doi: 10.3788/PI.2023.R01

[3] Huang K, Qin F, Liu H, et al. Planar diffractive lenses: fundamentals, functionalities, and applications. Advanced Materials. 2018;30:1704556. doi: 10.1002/adma.201704556

[4] Banerji S, Meem M, Majumder A, et al. Imaging with flat optics: metalenses or diffractive lenses? Optica. 2019;6:805. doi: 10.1364/OPTICA.6.000805

[5] Khorasaninejad M, Chen WT, Devlin RC, et al. Metalenses at visible wavelengths: diffraction-limited focusing and subwavelength resolution imaging. Science. 2016;352:1190–1194. doi: 10.1126/science.aaf6644

[6] Barulin A, Barulina E, Oh DK, et al. Axially multifocal metalens for 3D volumetric photoacoustic imaging of neuromelanin in live brain organoid. Sci Adv. 2025;11:eadr0654. doi: 10.1126/sciadv.adr0654

[7] Noh J, Cho H, Park C, et al. MetaCraft: database-driven metalens design and optimization software. SoftwareX. 2024;28:101954. doi: 10.1016/j.softx.2024.101954

[8] Zhang L, Chang S, Chen X, et al. High-efficiency, 80 mm aperture metalens telescope. Nano Lett. 2023;23:51–57. doi: 10.1021/acs.nanolett.2c03561

[9] Majumder A, Meem M, Ingold A, et al. Color astrophotography with a 100 mm-diameter f/2 polymer flat lens. Applied Physics Letters. 2025;126:051701. doi: 10.1063/5.0242208

[10] Park J-S, Lim SWD, Amirzhan A, et al. All-glass 100 mm diameter visible metalens for imaging the cosmos. ACS Nano. 2024;18:3187–3198. doi: 10.1021/acsnano.3c09462

[11] Arbabi A, Horie Y, Ball AJ, et al. Subwavelength-thick lenses with high numerical apertures and large efficiency based on high-contrast transmitarrays. Nat Commun. 2015;6:7069. doi: 10.1038/ncomms8069

[12] Khorasaninejad M, Shi Z, Zhu AY, et al. Achromatic metalens over 60 nm bandwidth in the visible and metalens with reverse chromatic dispersion. Nano Lett. 2017;17:1819–1824. doi: 10.1021/acs.nanolett.6b05137

[13] Moon S, Kim S, Kim J, et al. Single-layer waveguide displays using achromatic metagratings for full-colour augmented reality. Nat Nanotechnol. 2025;20:747–754. doi: 10.1038/s41565-025-01887-3

[14] Chang S, Zhang L, Duan Y, et al. Achromatic metalenses for full visible spectrum with extended group delay control via dispersion-matched layers. Nat Commun. 2024;15:9627. doi: 10.1038/s41467-024-53701-8

[15] Balli F, Sultan MA, Ozdemir A, et al. An ultrabroadband 3D achromatic metalens. Nanophotonics. 2021;10:1259–1264. doi: 10.1515/nanoph-2020-0550

[16] Wang S, Wu PC, Su V-C, et al. A broadband achromatic metalens in the visible. Nature Nanotech. 2018;13:227–232. doi: 10.1038/s41565-017-0052-4

[17] Chu Y, Xiao X, Ye X, et al. Design of achromatic hybrid metalens with secondary spectrum correction. Opt Express. 2023;31:21399. doi: 10.1364/OE.493216

[18] Li H, Xiao X, Fang B, et al. Bandpass-filter-integrated multiwavelength achromatic metalens. Photon Res. 2021;9:1384. doi: 10.1364/PRJ.422280

[19] Shrestha S, Overvig AC, Lu M, et al. Broadband achromatic dielectric metalenses. Light Sci Appl. 2018;7:85. doi: 10.1038/s41377-018-0078-x

[20] Zhao F, Zhao C, Zhang Y, et al. Centimeter-size achromatic metalens in long-wave infrared. Nanophotonics. 2025;14:589–599. doi: 10.1515/nanoph-2024-0716

[21] Wang Y, Chen Q, Yang W, et al. High-efficiency broadband achromatic metalens for near-IR biological imaging window. Nat Commun. 2021;12:5560. doi: 10.1038/s41467-021-25797-9

[22] Baek S, Kim J, Kim Y, et al. High numerical aperture RGB achromatic metalens in the visible. Photon Res. 2022;10:B30. doi: 10.1364/PRJ.470004

[23] Engelberg J, Levy U. Achromatic flat lens performance limits. Optica. 2021;8:834. doi: 10.1364/OPTICA.422843

[24] Liang H, Martins A, Borges B-HV, et al. High performance metalenses: numerical aperture, aberrations, chromaticity, and trade-offs. Optica. 2019;6:1461. doi: 10.1364/OPTICA.6.001461

[25] Presutti F, Monticone F. Focusing on bandwidth: achromatic metalens limits. Optica. 2020;7:624. doi: 10.1364/OPTICA.389404

[26] Wang Y, Fan Q, Xu T. Design of high efficiency achromatic metalens with large operation bandwidth using bilayer architecture. OEA. 2021;4:200008. doi: 10.29026/oea.2021.200008

[27] Li M, Li S, Chin LK, et al. Dual-layer achromatic metalens design with an effective abbe number. Opt. Express. 2020;28:26041. doi: 10.1364/OE.402478

[28] O'Shea DC, Suleski TJ, Kathman AD, et al. Diffractive optics: design, fabrication, and test. Bellingham, WA: SPIE press; 2003. doi: 10.1117/3.527861

[29] Sinzinger S, Testorf M. Transition between diffractive and refractive micro-optical components. Applied optics. 1995;34:5970–5976. doi: 10.1364/AO.34.005970

[30] Hazra L. Diffractive optical elements: past, present, and future (Vol. 3729) SPIE; 1999. pp. 198–211.

[31] Wang J, Deng Y, Wang C, et al. Portable astronomical observation system based on large-aperture concentric-ring metalens. Light Sci Appl. 2025;14:2. doi: 10.1038/s41377-024-01656-2

[32] Shi C, Zhao W, Chen S, et al. Multilevel diffractive lenses: recent advances and applications. Symmetry. 2024;16:1377. doi: 10.3390/sym16101377
[33] Swanson G1989. The theory and design of multi-level diffractive optical elements, MIT Technical Report 854.
[34] Yoon Y. Design and tolerancing of achromatic and anastigmatic diffractive–refractive lens systems compared with equivalent conventional lens systems. Appl Opt. 2000;39:2551. doi: 10.1364/AO.39.002551
[35] Flores A, Wang MR, Yang JJ. Achromatic hybrid refractive-diffractive lens with extended depth of focus. Appl Opt. 2004;43:5618. doi: 10.1364/AO.43.005618
[36] Greisukh GI, Ezhov EG, Stepanov SA. Diffractive-refractive hybrid corrector for achro- and apochromatic corrections of optical systems. Appl Opt. 2006;45:6137. doi: 10.1364/AO.45.006137
[37] Schmid M, Sterl F, Thiele S, et al. 3D printed hybrid refractive/diffractive achromat and apochromat for the visible wavelength range. Opt Lett. 2021;46:2485. doi: 10.1364/OL.423196
[38] Richards CA, Ocier CR, Xie D, et al. Hybrid achromatic microlenses with high numerical apertures and focusing efficiencies across the visible. Nat Commun. 2023;14:3119. doi: 10.1038/s41467-023-38858-y
[39] Sweeney DW, Sommargren GE. Harmonic diffractive lenses. Applied Optics. 1995;34:2469–2475. doi: 10.1364/AO.34.002469
[40] Ivliev N, Evdokimova V, Podlipnov V, et al. First earth-imaging cubesat with harmonic diffractive lens. Remote Sensing. 2022;14:2230. doi: 10.3390/rs14092230
[41] Wang P, Mohammad N, Menon R. Chromatic-aberration-corrected diffractive lenses for ultra-broadband focusing. Scientific Reports. 2016;6:1–7.
[42] Pan M, Fu Y, Zheng M, et al. Dielectric metalens for miniaturized imaging systems: progress and challenges. Light Sci Appl. 2022;11:195. doi: 10.1038/s41377-022-00885-7
[43] So S, Mun J, Park J, et al. Revisiting the design strategies for metasurfaces: fundamental physics, optimization, and beyond. Advanced Materials. 2023;35:2206399. doi: 10.1002/adma.202206399
[44] Yang Y, Kang H, Jung C, et al. Revisiting optical material platforms for efficient linear and nonlinear dielectric metasurfaces in the ultraviolet, visible, and infrared. ACS Photonics. 2023;10:307–321. doi: 10.1021/acsphotonics.2c01341
[45] Chen WT, Zhu AY, Capasso F. Flat optics with dispersion-engineered metasurfaces. Nat Rev Mater. 2020;5:604–620. doi: 10.1038/s41578-020-0203-3
[46] Peng Y, Zhang J, Zhou X, et al. Metalens in improving imaging quality: advancements, challenges, and prospects for future display. Laser Photonics Reviews. 2024;18:2300731. doi: 10.1002/lpor.202300731
[47] Banerji S, Meem M, Majumder A, et al. Extreme-depth-of-focus imaging with a flat lens. Optica. 2020;7:214–217. doi: 10.1364/OPTICA.384164
[48] Zhou F, Zhou F, Chen Y, et al. Vector light field display based on an intertwined flat lens with large depth of focus. Optica. 2022;9:288–294. doi: 10.1364/OPTICA.439613
[49] Lin D, Hayward TM, Jia W, et al. Inverse-designed multi-level diffractive doublet for wide field-of-view imaging. ACS Photonics. 2023;10:2661–2669. doi: 10.1021/acsphotonics.3c00406
[50] Pinilla S, Fröch JE, Miri Rostami SR, et al. Miniature color camera via flat hybrid meta-optics. Science Advances. 2023;9:eadg7297. doi: 10.1126/sciadv.adg7297
[51] Seldowitz MA, Allebach JP, Sweeney DW. Synthesis of digital holograms by direct binary search. Applied optics. 1987;26:2788–2798. doi: 10.1364/AO.26.002788
[52] Hooke R, Jeeves TA. "Direct Search" solution of numerical and statistical problems. Journal of the ACM (JACM). 1961;8:212–229. doi: 10.1145/321062.321069
[53] Fan Y, Chen MK, Qiu M, et al. Experimental demonstration of genetic algorithm based metalens design for generating side-lobe-suppressed, large depth-of-focus light sheet. Laser Photonics Reviews. 2022;16:2100425. doi: 10.1002/lpor.202100425
[54] Haupt RL, Werner DH. Genetic Algorithms in Electromagnetics. John Wiley & Sons; 2007.
[55] Shi C, Wang Y, Liu Q, et al. Inverse design on terahertz multilevel diffractive lens based on 3D printing. Chin Opt Lett. 2023;21:110006. doi: 10.3788/COL202321.110006
[56] Xiao X, Zhao Y, Ye X, et al. Large-scale achromatic flat lens by light frequency-domain coherence optimization. Light Sci Appl. 2022;11:323. doi: 10.1038/s41377-022-01024-y
[57] Lin Z, Roques-Carmes C, Christiansen RE, et al. Computational inverse design for ultra-compact single-piece metalenses free of chromatic and angular aberration. Applied Physics Letters. 2021;118:041104. doi: 10.1063/5.0035419
[58] Chung H, Miller OD. High-NA achromatic metalenses by inverse design. Opt Express. 2020;28:6945. doi: 10.1364/OE.385440
[59] Roques-Carmes C, Lin Z, Christiansen RE, et al. Toward 3D-printed inverse-designed metaoptics. ACS Photonics. 2022;9:43–51. doi: 10.1021/acsphotonics.1c01442
[60] Jiang Q, Liu J, Li J, et al. Multiwavelength achromatic metalens in visible by inverse design. Advanced Optical Materials. 2023;11:2300077. doi: 10.1002/adom.202300077
[61] Jin Z, Lin Y, Wang C, et al. Topologically optimized concentric-nanoring metalens with 1 mm diameter, 0.8 NA and 600 nm imaging resolution in the visible. Opt Express. 2023;31:10489. doi: 10.1364/OE.478680
[62] Wang C, Lin Y, Han Y, et al. Fabricable concentric-ring metalens with high focusing efficiency based on two-dimensional subwavelength unit splicing. Opt Express. 2023;31:33596. doi: 10.1364/OE.500688

[63] Engelberg J, Levy U. Standardizing flat lens characterization. Nature Photonics. 2022;16:171–173. doi: 10.1038/s41566-022-00963-7
[64] Peng Y, Fu Q, Heide F, et al. The diffractive achromat full spectrum computational imaging with diffractive optics. ACM Trans Graph. 2016;35:1–11.
[65] Mohammad N, Meem M, Shen B, et al. Broadband imaging with one planar diffractive lens. Scientific Reports. 2018;8:1–6. doi: 10.1038/s41598-018-21169-4
[66] Meem M, Majumder A, Menon R. Full-color video and still imaging using two flat lenses. Optics Express. 2018;26:26866–26871. doi: 10.1364/OE.26.026866
[67] Meem M, Banerji S, Majumder A, et al. Inverse-designed achromatic flat lens enabling imaging across the visible and near-infrared with diameter> 3 mm and NA= 0.3. Applied Physics Letters. 2020;117:041101. doi: 10.1063/5.0012759
[68] Doskolovich LL, Skidanov RV, Bezus EA, et al. Design of diffractive lenses operating at several wavelengths. Optics Express. 2020;28:11705–11720. doi: 10.1364/OE.389458
[69] Yang G, Zhang F, Pu M, et al. Dual-wavelength multilevel diffractive lenses for near-infrared imaging. J Phys D: Appl Phys. 2021;54:175109. doi: 10.1088/1361-6463/abe07d
[70] Meem M, Banerji S, Majumder A, et al. Broadband lightweight flat lenses for long-wave infrared imaging. Proceedings of the National Academy of Sciences. 2019;116:21375–21378. doi: 10.1073/pnas.1908447116
[71] Meem M, Majumder A, Banerji S, et al. Imaging from the visible to the longwave infrared wavelengths via an inverse-designed flat lens. Optics Express. 2021;29:20715–20723. doi: 10.1364/OE.423764
[72] Yildırım BK, Kurt H, Turduev M. Ultra-compact, high-numerical-aperture achromatic multilevel diffractive lens via metaheuristic approach. Photonics Research. 2021;9:2095–2103. doi: 10.1364/PRJ.427523
[73] Pan C-F, Wang H, Wang H, et al. 3D-printed multilayer structures for high–numerical aperture achromatic metalenses. Sci Adv. 2023;9:eadj9262. doi: 10.1126/sciadv.adj9262
[74] Born M, Wolf E. Principles of Optics. 7th ed. Cambridge University Press; 1999.
[75] Li X, Meng F, Chen Y, et al. Designer graphene oxide ultrathin flat lens with versatile focusing property. Opt Express. 2024;32:6531. doi: 10.1364/OE.509599
[76] Cao G, Wei S, Wang S, et al. Multi-wavelength achromatic graphene metalenses for visible, NIR, and beyond. Laser Photonics Reviews. 2025;19:2401542. doi: 10.1002/lpor.202401542
[77] Choi M, Kim J, Moon S, et al. Roll-to-plate printable RGB achromatic metalens for wide-field-of-view holographic near-eye displays. Nat Mater. 2025;24:535–543. doi: 10.1038/s41563-025-02121-0
[78] Zu X, Sun X, Yan W, et al. Fast and efficient inverse design framework for multifunctional metalenses. Laser Photonics Reviews. 2025;19:2400886. doi: 10.1002/lpor.202400886
[79] Khaidarov E, Eschimese D, Lai KH, et al. Large-scale vivid metasurface color printing using advanced 12-in. immersion photolithography. Sci Rep. 2022;12:14044. doi: 10.1038/s41598-022-18259-9
[80] Sun Q, Tseng E, Fu Q, et al. Learning Rank-1 diffractive optics for single-shot high dynamic range imaging. IEEE/CVF Conference on Computer Vision and Pattern Recognition (CVPR). 2020;1383–1393. doi: 10.1109/CVPR42600.2020.00146
[81] Seo J, Jo J, Kim J, et al. Deep-learning-driven end-to-end metalens imaging. Adv Photon. 2024;6:066002. doi: 10.1117/1.AP.6.6.066002
[82] Chi H, Hu Y, Ou X, et al. Neural network-assisted end-to-end design for full light field control of meta-optics. Advanced Materials. 2025;37:2419621. doi: 10.1002/adma.202419621
[83] Peng Y, Sun Q, Dun X, et al. Learned large field-of-view imaging with thin-plate optics. ACM Trans Graph. 2019;38:219–211. doi: 10.1145/3355089.3356526
[84] Heide F, Fu Q, Peng Y, et al. Encoded diffractive optics for full-spectrum computational imaging. Sci Rep. 2016;6:33543. doi: 10.1038/srep33543
[85] Kanmaz TB, Ozturk E, Demir HV, et al. Deep-learning-enabled electromagnetic near-field prediction and inverse design of metasurfaces. Optica. 2023;10:1373. doi: 10.1364/OPTICA.498211
[86] Peng Y, Fu Q, Amata H, et al. Computational imaging using lightweight diffractive-refractive optics. Opt Express, OE. 2015;23:31393–31407. doi: 10.1364/OE.23.031393
[87] Nikonorov A, Evdokimova V, Petrov M, et al. Deep learning-based imaging using single-lens and multi-aperture diffractive optical systems. IEEE/CVF International Conference on Computer Vision Workshop (ICCVW). 2019;3969–3977. doi: 10.1109/ICCVW.2019.00491
[88] Liu X, Li L, Liu X, et al. Investigating deep optics model representation in affecting resolved all-in-focus image quality and depth estimation fidelity. Opt Express, OE. 2022;30:36973–36984. doi: 10.1364/OE.473084
[89] Dong Y, Zheng B, Li H, et al. Achromatic single metalens imaging via deep neural network. ACS Photonics. 2024;11:1645–1656. doi: 10.1021/acsphotonics.3c01870
[90] Fröch JE, Chakravarthula P, Sun J, et al. Beating spectral bandwidth limits for large aperture broadband nano-optics. Nat Commun. 2025;16:3025. doi: 10.1038/s41467-025-58208-4
[91] Chakravarthula P, Sun J, Li X, et al. Thin on-sensor nanophotonic array cameras. ACM Trans. Graph. 2023;42:1–18. doi: 10.1145/3618398
[92] Tseng E, Colburn S, Whitehead J, et al. Neural nano-optics for high-quality thin lens imaging. Nature communications. 2021;12:1–7. doi: 10.1038/s41467-021-26443-0

[93] Zhang P, Yan L, Liang H, et al. RGB achromatic metalens for neural network-enhanced high resolution digital imaging. Laser Photonics Reviews. 2025;19(18):e00460. doi: 10.1002/lpor.202500460
[94] Hu S, Xiao X, Ye X, et al. Deep learning enhanced achromatic imaging with a singlet flat lens. Opt Express, OE. 2023;31:33873–33882. doi: 10.1364/OE.501872
[95] Maman R, Mualem E, Mazurski N, et al. Achromatic imaging systems with flat lenses enabled by deep learning. ACS Photonics. 2023;10:4494–4500. doi: 10.1021/acsphotonics.3c01349
[96] Evdokimova VV, Podlipnov VV, Ivliev NA, et al. Hybrid refractive-diffractive lens with reduced chromatic and geometric aberrations and learned image reconstruction. Sensors. 2023;23:415. doi: 10.3390/s23010415
[97] Zhong X, Wang H, Liu Z, et al. End-to-end learned diffractive imaging system lithography adaptation design using hierarchical-dynamic simulation. Opt Lett, OL. 2025;50:2812–2815. doi: 10.1364/OL.557427
[98] Pei X, Yu X, Gao X, et al. "End-to-end optimization of a diffractive optical element and aberration correction for integral imaging,". Chin Opt Lett. 2022;COL 20:121101.
[99] Dun X, Ikoma H, Wetzstein G, et al. Learned rotationally symmetric diffractive achromat for full-spectrum computational imaging. Optica, OPTICA. 2020;7:913–922. doi: 10.1364/OPTICA.394413
[100] Sun Q, Zhang J, Dun X, et al. End-to-end learned, optically coded super-resolution SPAD camera. ACM Trans Graph. 2020;39:1–14. doi: 10.1145/3372261
[101] Sitzmann V, Diamond S, Peng Y, et al. End-to-end optimization of optics and image processing for achromatic extended depth of field and super-resolution imaging. ACM Trans Graph. 2018;37:1–13. doi: 10.1145/3197517.3201333
[102] Zhang J, Zhao Z, Fan Z, et al. Hybrid design scheme for enabling large-aperture diffractive achromat imaging. Opt Express, OE. 2024;32:28402–28412. doi: 10.1364/OE.525558
[103] Jia W, Lin D, Menon R, et al. Machine learning enables the design of a bidirectional focusing diffractive lens. Opt Lett, OL. 2023;48:2425–2428. doi: 10.1364/OL.489535
[104] Jia W, Lin D, Menon R, et al. Multifocal multilevel diffractive lens by wavelength multiplexing. Appl Opt, AO. 2023;62:6931–6938. doi: 10.1364/AO.497775
[105] Zhang Y, Song X, Xie J, et al. Large depth-of-field ultra-compact microscope by progressive optimization and deep learning. Nat Commun. 2023;14:4118. doi: 10.1038/s41467-023-39860-0
[106] Colburn S, Zhan A, Majumdar A. Metasurface optics for full-color computational imaging. Science Advances. 2018;4:eaar2114. doi: 10.1126/sciadv.aar2114
[107] Thiele S, Pruss C, Herkommer AM, et al. 3D printed stacked diffractive microlenses. Opt Express. 2019;27:35621. doi: 10.1364/OE.27.035621
[108] Li Y, Yu Y, Guo L, et al. High efficiency multilevel phase-type Fresnel zone plates produced by two-photon polymerization of SU-8. J Opt. 2010;12:035203. doi: 10.1088/2040-8978/12/3/035203
[109] Wu D, Niu L-G, Chen Q-D, et al. High efficiency multilevel phase-type fractal zone plates. Opt Lett. 2008;33:2913. doi: 10.1364/OL.33.002913
[110] Vanmol K, Abdul Nazar AA, Thienpont H, et al. Fabrication of multilevel metalenses using multiphoton lithography: from design to evaluation. Opt Express. 2024;32:10190. doi: 10.1364/OE.514237
[111] Balli F, Sultan M, Lami SK, et al. A hybrid achromatic metalens. Nat Commun. 2020;11:3892. doi: 10.1038/s41467-020-17646-y
[112] Aguiam DE, Santos JD, Silva C, et al. Fabrication and optical characterization of large aperture diffractive lenses using greyscale lithography. Micro and Nano Engineering. 2022;14:100111. doi: 10.1016/j.mne.2022.100111
[113] Li J, Ge S, Liu W. High-efficiency and high-precision replication manufacturing of large-aperture multi-level diffractive lenses In: Jiang Y, Wang X, Cao L, Wang Q-H, Liu D, Xue B, Wang Y, Lu C-Y, editors. AOPC 2023: Optical Sensing, Imaging, and Display Technology and Applications; and Biomedical Optics. SPIE; 2023. p. 66.
[114] Britton WA, Chen Y, Sgrignuoli F, et al. Compact dual-band multi-focal diffractive lenses. Laser Photonics Reviews. 2021;15:2000207. doi: 10.1002/lpor.202000207
[115] Hao C, Gao S, Ruan Q, et al. Single-layer aberration-compensated flat lens for robust wide-angle imaging. Laser Photonics Reviews. 2020;14:2000017. doi: 10.1002/lpor.202000017
[116] Duan H, Wang M, Hu X, et al. Aberration-compensated supercritical lens for sub-diffractive focusing within 20° field of view. Opt Lett. 2023;48:2523. doi: 10.1364/OL.489652
[117] Reda F, Salvatore M, Borbone F, et al. Varifocal diffractive lenses for multi-depth microscope imaging. Opt Express. 2022;30:12695. doi: 10.1364/OE.455520
[118] Rostami SRM, Katkovnik V, Egiazarian K. Extended DoF and achromatic inverse imaging for lens and lensless MPM camera based on wiener filtering of defocused OTFs. Opt Eng. 2021;60. doi: 10.1117/1.OE.60.5.051204
[119] Hadibrata W, Wei H, Krishnaswamy S, et al. Inverse Design and 3d Printing of a Metalens on an Optical Fiber Tip for Direct Laser Lithography. Nano Lett. 2021;21:2422–2428. doi: 10.1021/acs.nanolett.0c04463